# Kinematics of the west-central Walker Lane: Spatially and temporally variable rotations evident in the Late Miocene Stanislaus Group

**Chad W. Carlson[1,*], Christopher J. Pluhar[1], Jonathan M.G. Glen[2], and Michael J. Farner[1,*]**
[1]*Department of Earth and Environmental Sciences, California State University–Fresno, 2576 East San Ramon Avenue, M/S ST24, Fresno, California 93740, USA*
[2]*Geophysical Unit Menlo Park (GUMP), U.S. Geological Survey, 345 Middlefield Road, MS989, Menlo Park, California 94025, USA*

## ABSTRACT

**The Walker Lane currently accommodates ~20% of the dextral motion between the Pacific and North American plates. This accommodation occurs on regional-scale systems of strike-slip and normal faults located between the northwestward-translating Sierra Nevada microplate and the east-west–extending Basin and Range. At the western edge of the central Walker Lane (lat ~38°–39°N) is a region of crustal blocks bounded by asymmetric basins and normal faults, here defined as the west-central Walker Lane. Although this region is apparently devoid of major active strike-slip faults, the presence of Neogene clockwise vertical-axis tectonic block rotations indicates the accommodation of dextral shear. We measured vertical-axis rotation by comparing remanence directions of widespread members of the Eureka Valley Tuff of the Late Miocene Stanislaus Group within the west-central Walker Lane to the same units on the Sierra Nevada microplate.**

**Results show that the study area is organized into discrete domains with heterogeneous regional distribution of clockwise vertical-axis rotation, ranging from ~10° to 60°, since ca. 9.5 Ma. The highest measured magnitudes of vertical-axis rotation (~50°–60° clockwise) are interpreted as a region of high deformation that includes the asymmetric Bridgeport Valley. Previous work underestimated vertical-axis rotation magnitudes in the region because published reference directions for two of the three members of the Eureka Valley Tuff (By-Day Member and Upper member) derive from the rotated region. We recalculate a reference direction for the By-Day Member of declination 353.2°, inclination 43.7°; $\alpha_{95}$ = 10.8°. This corroborates a reference direction for the By-Day Member from the Stanislaus Group type section, situated on the relatively stable Sierra Nevada microplate, providing a robust reference direction for paleomagnetic studies. We present a kinematic model in which dextral shear in the west-central Walker Lane is accommodated by ~30° of clockwise rotation in the Sweetwater Mountains and Bodie Hills since the Late Miocene. This model incorporates rotation magnitudes, paleostress orientations, edge effects, and bounding faults of rotating tectonic blocks to reveal timing, patterns, and mechanisms of crustal deformation.**

**The results and models presented here elucidate the complex and evolving nature of the west-central Walker Lane. The rotational history of dextral shear accommodation demonstrates that the west-central Walker Lane should be included as an important part of the Walker Lane transtensional zone. The results presented in this study not only improve understanding of deformation in the Walker Lane, but illuminate the potentially significant contribution of crustal block vertical-axis rotations in other transtensional regions of the world.**

## INTRODUCTION

Plate boundaries are classically defined as discrete zones of faulting. Due to the relative weakness of felsic crust, this description often falls short of characterizing continental plate boundaries, which can be exceptionally complex with broad regions of deformation (e.g., Gordon, 1995; Thatcher, 1995). Such distributed plate boundary zones often exhibit regions of crustal block rotations about a vertical axis (e.g., England and Wells, 1991; Lamb, 1994; Allmendinger, 2007). The Pacific–North American plate boundary extends from the continental margin, through the San Andreas fault system and eastward for hundreds of kilometers across western North America (Dixon et al., 1995, 2000, 2003; Miller et al., 2001; Oldow et al., 2001; Oldow, 2003; Faulds et al., 2005). This broad zone of deformation is distributed onto numerous, and sometimes disparate and discontinuous, fault systems and has undergone extensive vertical-axis rotation in some areas (e.g., Cashman and Fontaine, 2000; Faulds and Perkins, 2007; Petronis et al., 2009; Rood et al., 2011).

The Walker Lane currently accommodates ~20% of the dextral motion between the North American and Pacific plates on systems of strike-slip and normal faulting (Dixon et al., 1995, 2000; Kreemer et al., 2009; Fig. 1). Positioned between the Basin and Range extensional province and the Sierra Nevada microplate, the Walker Lane is a north-northwest–striking region of complex physiography and transtensional deformation (e.g., Stewart, 1988; Oldow, 2003; Faulds and Henry, 2008; Fig. 1). However, some regions within and/or adjacent to the Walker Lane that do not currently display major strike-slip faults or significant oblique slip on normal faults may be overlooked as contributing regions to Walker Lane dextral shear accommodation. An understanding of how, when, and where dextral motion is and has been accommodated in the Walker Lane is integral to understanding the evolution of this portion of western North America.

*Present addresses: Carlson: Department of Geological Sciences and Engineering, University of Nevada–Reno, 1664 N. Virginia Street, Reno, Nevada 89557-0172, USA; Farner: Department of Earth Science, Rice University, 6100 Main Street, MS-126, Houston, Texas 77005, USA.

*Geosphere*; December 2013; v. 9; no. 6; p. 1530–1551; doi:10.1130/GES00955.1; 11 figures; 4 tables.
Received 4 June 2013 ♦ Revision received 8 September 2013 ♦ Accepted 11 October 2013 ♦ Published online 13 November 2013

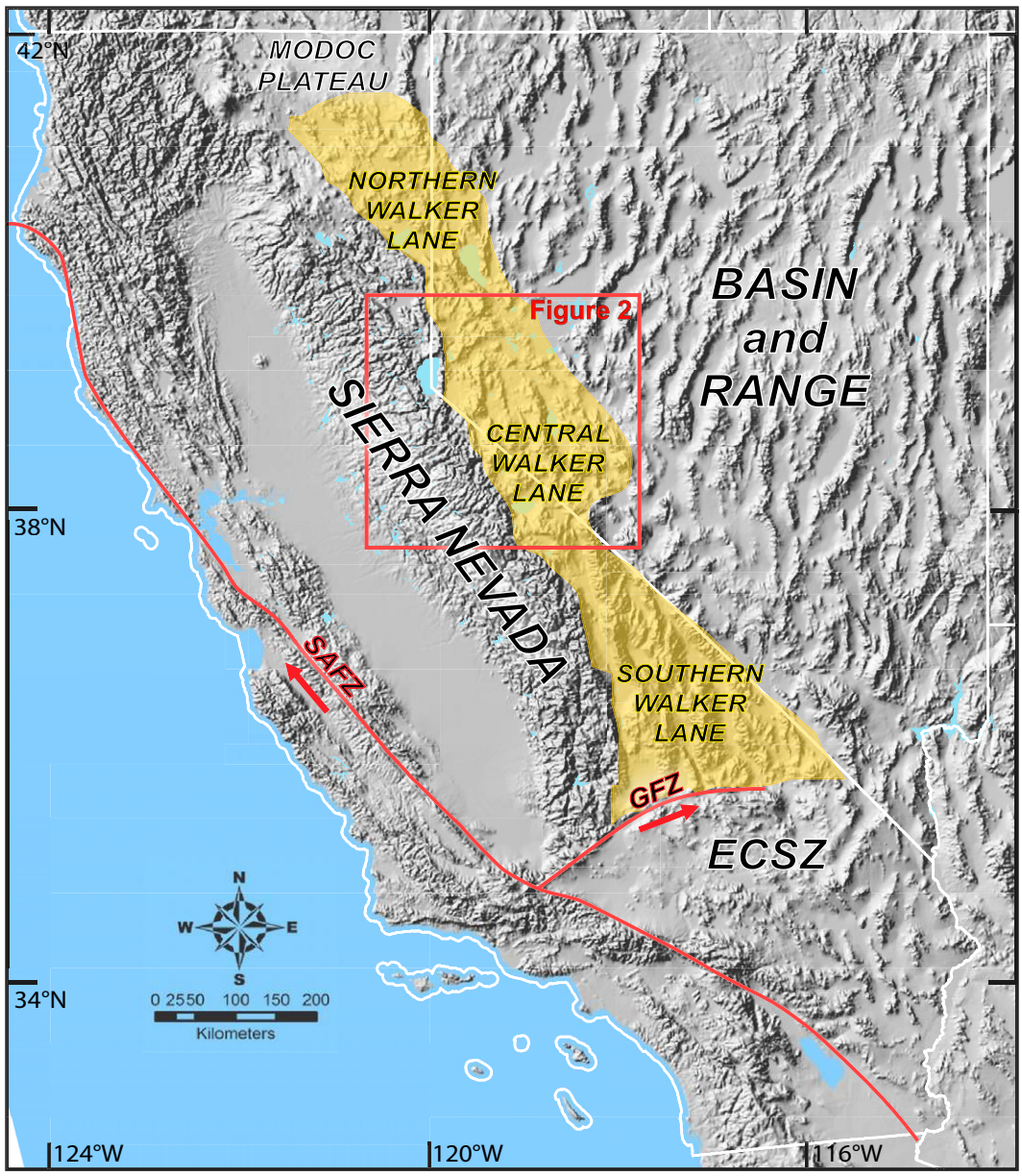


**Figure 1. Shaded relief map depicting a portion of western North America. California and Nevada state boundaries are outlined in white; yellow indicates the extent of the Walker Lane as defined in this study. ECSZ—Eastern California shear zone; SAFZ—San Andreas fault zone; GFZ—Garlock fault zone.**

In the western portion of the central Walker Lane, topographic highs are distributed among present-day normal fault–bounded depositional basins (Fig. 2). Inclusion of this region as part of the Walker Lane has varied among researchers (e.g., Locke et al., 1940; Hardyman, 1984; Stewart, 1988; Wesnousky, 2005; Faulds and Henry, 2008; Surpless, 2008). This region, herein called the west-central Walker Lane, extends eastward from the Sierran frontal fault system demarcating the eastern boundary of the Sierra Nevada microplate, to the frontal fault bounding the east side of the Wassuk Range and sinistral faults of the Mina deflection; and northward from Mono Lake to the southern edge of Stewart's (1988) Carson domain and the Wabuska lineament (Fig. 2). Crustal blocks draped by late Cenozoic volcanics in this region present an opportunity to examine the interplay of regional dextral shear and western encroachment of tectonic activity into the Sierra Nevada microplate.

Volcanic rocks provide an excellent record of Earth's magnetic field at the time of their emplacement. In addition, the magnetization of widely distributed units, such as welded tuffs, can be used to resolve the sense and magnitudes of relative motions between discrete tectonic blocks over a large area. With the southern edge of the subducting Gorda plate inferred to have been near the latitude of the study region (~38°N) ca. 10 Ma (e.g., Atwater and Stock, 1998; Jones et al., 2004), the Late Miocene Eureka Valley Tuff of the Stanislaus Group provides an ideal spatial and temporal marker for geologic events subsequent to the Mendocino Triple Junction passage and transition from an oblique convergent to transform plate boundary. The vast areal distribution of these volcanic rocks provides the means for mapping out variations in paleomagnetic directions between units deposited within the Walker Lane and those same lithologies deposited on the more tectonically stable Sierra Nevada microplate.

The previous use of paleomagnetism for interpreting crustal kinematics has substantially improved understanding of dextral shear accommodation in portions of the Walker Lane

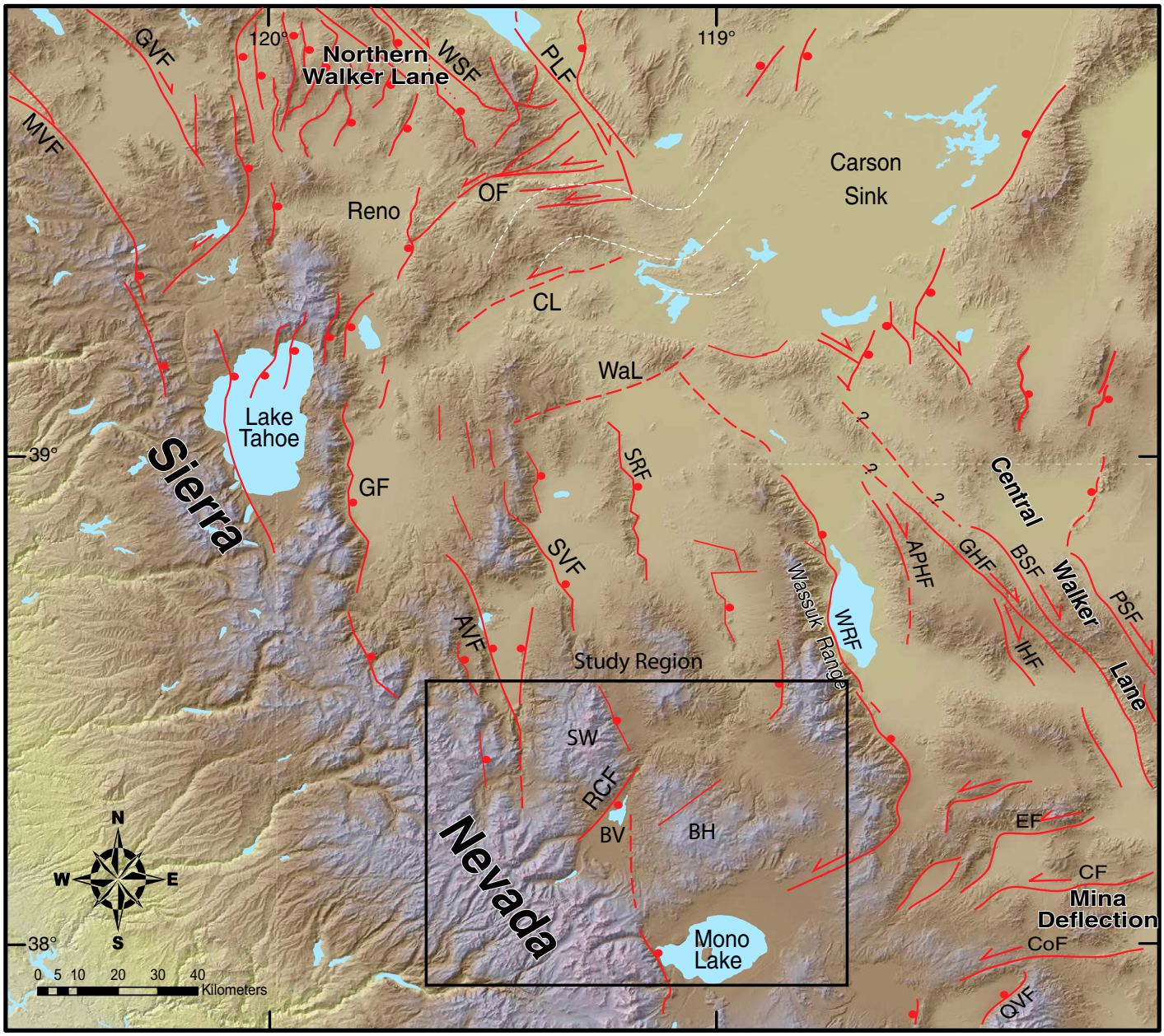


**Figure 2. Colored shaded-relief map of portions of the northern and central Walker Lane. Major faults and lineaments are modified from Faulds and Henry (2008). Physiographic study regions: BH—Bodie Hills; BV—Bridgeport Valley; SW—Sweetwater Mountains. Regional faults: APHF—Agai Pai Hills fault; AVF—Antelope Valley fault; BSF—Benton Springs fault; CF—Candelaria fault; CL—Carson lineament; CoF—Coaldale fault; EF—Excelsior fault; GF—Genoa fault; GHF—Gumdrop Hills fault; GVF—Grizzly Valley fault; IHF—Indian Head fault; MVF—Mohawk Valley fault; OF—Olinghouse fault; PLF—Pyramid Lake fault; PSF—Petrified Springs fault; QVF—Queen Valley fault; RCF—Robinson Creek fault; SRF—Singatse Range fault; SVF—Smith Valley fault; Wal—Wabuska lineament; WRF—Wassuk Range frontal fault; WSF—Warm Springs Valley fault. White dashed lines denote orocline of Faulds and Henry (2008).**

(Cashman and Fontaine, 2000; King et al., 2007; Pluhar et al., 2006; Lewis et al., 2007; Ferranti et al., 2009; Petronis et al., 2009; Rood et al., 2011). We similarly apply paleomagnetic techniques to identify vertical-axis rotations of tectonic blocks in the west-central Walker Lane. The presence of vertical-axis rotations is representative of components of dextral shearing in this region and validates west-central Walker Lane inclusion as part of the greater Walker Lane. Also, dense kinematic data across this wide region, apparently devoid of prominent and active strike-slip structures, advance an understanding of shear accommodation within the central Walker Lane and can contribute to broader understanding of the role of vertical-axis rotation in other transform systems.

Paleomagnetically determined vertical-axis rotations in the west-central Walker Lane provide long time-averaged rotation rates from the time of unit emplacement. Much of the

documented present-day west-central Walker Lane regional deformation, based on Holocene fault displacement and seismic data, is predominantly dip-slip motion and seems inconsistent with accommodating large magnitudes of vertical-axis rotation in the absence of significant oblique-slip components (e.g., Clark et al., 1984; Hayes, 1985; Unruh et al., 2003). In addition, geodetic models using short-term averages (e.g., McCaffrey, 2002; Hammond et al., 2011) have predicted present-day vertical-axis rotation rates lower than paleomagnetically derived rates in this region (King et al., 2007; Rood et al., 2011). This difference between long-term paleomagnetically derived vertical-axis rotation rates with those inferred from present-day geologic and geodetic measurements may reflect a regional change in deformation style since the Late Miocene.

In this paper we document that a portion of the west-central Walker Lane has accommodated north-northwest motion of the Sierra Nevada microplate relative to the Basin and Range, and did so by crustal block vertical-axis rotations. This study utilizes ~300 newly acquired paleomagnetic samples from Stanislaus Group rocks, in combination with reinterpreted results from previous studies, to examine tectonic vertical-axis rotation of 28 sampling localities. These data help to (1) characterize vertical-axis rotations and define domains of rotation in the west-central Walker Lane, (2) compare temporal evolution and deformation style between tectonic domains within and outside of the west-central Walker Lane, and (3) facilitate an understanding of block-rotation kinematics in the region. As part of these results, we identify rotations in portions of the study area previously believed to be unrotated. This is significant because (1) reference directions for two members of the Eureka Valley Tuff were derived from these rotated regions, and (2) identification of all regions accommodating dextral shear, past or present, is critical for the complete understanding of kinematics and strain partitioning within the Walker Lane. We propose a kinematic model for the evolution of a portion of the west-central Walker Lane across the transition zone from the Sierra Nevada frontal fault system eastward into the central Walker Lane since the Late Miocene. Our kinematic model takes into account not only vertical-axis rotations, but regional physiography, paleostress indicators, and changes in deformation over time. This study further illuminates the significant contribution that vertical-axis crustal block rotation plays in the accommodation of transform motion, not only within portions of the Walker Lane, but potentially other transform plate boundaries.

## GEOLOGIC SETTING AND TECTONIC FRAMEWORK

This section includes a brief overview of the Walker Lane and the study area as well as generalized stratigraphy of the Stanislaus Group near Sonora Pass, with focus on geologic units used for paleomagnetic analysis. Further detail of Stanislaus Group stratigraphy, ages, and geochemistry are readily available in the cited references (especially Slemmons, 1966; Noble et al., 1974; Busby et al., 2013a,). We present some of the methods and interpretations of previous workers used to gain a greater understanding of Walker Lane tectonics and dextral shear deformation.

### Walker Lane

The Pacific–North American transform plate boundary has lengthened and evolved over time through progressive migration of Mendocino and Rivera Triple Junctions to the north and south, respectively (Atwater and Stock, 1998). This ongoing reorganization of the plate boundary from a convergent to transform regime has resulted in the (1) creation of crustal microplates, such as remnant pieces of the Farallon plate along coastal California, and the Sierra Nevada microplate (Lonsdale, 1991; Nicholson et al., 1994; Dixon et al., 1995, 2000; Atwater and Stock, 1998; Argus and Gordon, 2001; Unruh et al., 2003); (2) a Middle-Late Miocene acceleration or jump in RTJ propagation ~1000 km to the south that was accompanied by the activation of inland dextral motion–accommodating structures (i.e., Walker Lane and Gulf of California; Oskin and Stock, 2003; Wesnousky, 2005; Faulds and Henry, 2008); (3) extensional collapse of the western North American Nevadaplano (Wernicke et al., 1988; Jones et al., 1996; DeCelles, 2004); and (4) increased volcanism in the western Basin and Range from the Oligocene ignimbrite flare-up to Quaternary basaltic lavas (e.g., Dickinson, 2006; Henry et al., 2010; John et al., 2012).

The Walker Lane has played an important role in plate boundary reorganization and accommodation of transform motion between the North American and Pacific plates. The western boundary of the Walker Lane is marked by the Sierra Nevada frontal fault system, characterized by discontinuous strands of east-down normal faults (e.g., Wakabayashi and Sawyer, 2001; Unruh et al., 2003). In contrast, dextral strike-slip faults predominantly bound the eastern edge of the Walker Lane, separating it from the Basin and Range province (e.g., Fish Lake Valley–Furnace Creek fault, Petrified and Benton Springs faults, and Pyramid Lake fault; southern to northern Walker Lane). The Walker Lane exhibits variations in kinematics and age of deformation along its length extending from the Eastern California shear zone at its southern end, to the Modoc Plateau at its northern terminus (Stewart, 1988; Faulds et al., 2005; Wesnousky, 2005; Faulds and Henry, 2008; Jayko and Bursik, 2012; Fig. 1). The more tectonically mature southern Walker Lane is characterized by continuous northwest-trending dextral-fault systems that extend for hundreds of kilometers (e.g., Owens Valley, Panamint Valley–Hunter Mountain–Saline Valley, Death Valley–Furnace Creek–Fish Lake Valley; Wesnousky, 2005; Faulds and Henry, 2008). In contrast, the northern Walker Lane consists of a system of faults with varying orientations and motions that have individual lengths of tens of kilometers (e.g., Pyramid Lake, Olinghouse, Warm Springs Valley, Honey Lake, and various north-northeast–striking normal faults; Wesnousky, 2005; Faulds and Henry, 2008). The central Walker Lane, characterized by disparate and discontinuous systems of dextral, sinistral, and normal faults, demarcates the significant shift in deformation style between the northern and southern Walker Lane and links the two across a releasing right step (Fig. 2).

The western portion of the central Walker Lane is composed of normal fault–bounded and volcanic-draped topographic highs interspersed among asymmetric wedge-shaped basins (Fig. 2). Located between the crest of the central Sierra Nevada and the northwestern edge of the Mina deflection, the Sweetwater Mountains and Bodie Hills bound the Bridgeport Valley to the northwest and east, respectively (Fig. 2). The Sweetwater Mountains are located directly east of a series of downdropped tectonic blocks forming the Sierran frontal fault system at the latitude of Sonora Pass (Busby et al., 2008, 2013b). The volcanics deposited on both the Sweetwater Mountains and Bodie Hills span ages from the Middle Miocene to the present, and compositions from mafic to felsic (Brem, 1984; John et al., 2012). Of the Neogene volcanics in the study area, four units are regional in nature; in ascending stratigraphic order, Valley Springs Formation, Relief Peak Formation, Stanislaus Group, and Disaster Peak Formation. Only lithologies of the Stanislaus Group provide a distinct stratigraphic marker clearly identifiable from the Sierra Nevada through the Sweetwater Mountains to the Bodie Hills.

### Stanislaus Group Stratigraphy

Volcanic lithologies of the Stanislaus Group are distributed from their sources eastward into the central Walker Lane, and extend as far west as Knights Ferry along the Stanislaus River in the central Sierran foothills (Fig. 3; Slemmons,

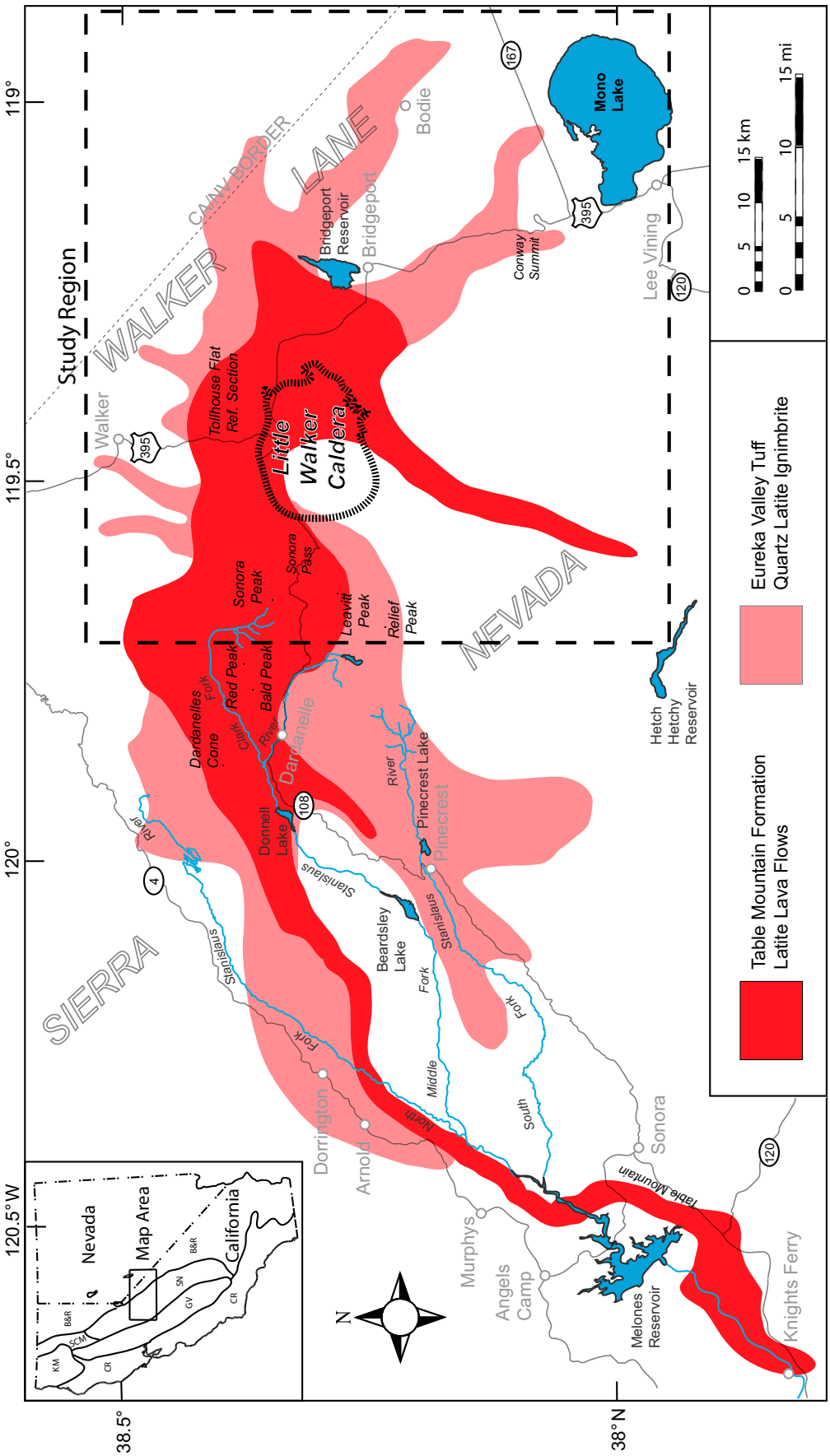


**Figure 3. Regional map showing distribution of the Table Mountain Formation and Eureka Valley Tuff Members of the Stanislaus Group (modified from King et al., 2007; Pluhar et al., 2009). Physiographic regions in inset: B&R—Basin and Range; CR—Coast Ranges; GV—Great Valley; KM—Klamath Mountains; SCM—southern Cascade Mountains; SN—Sierra Nevada.**

1953, 1966; Noble et al., 1974; Brem, 1984; John et al., 2012). The Stanislaus Group near Sonora Pass is composed of a series of lavas and ignimbrites erupted ca. 10.4–9.1 Ma (Busby et al., 2008; Pluhar et al., 2009; Farner et al., 2012). In ascending stratigraphic order, the Stanislaus Group consists of the Table Mountain Formation, the Eureka Valley Tuff, and the Dardanelles Formation (Fig. 4; Noble et al., 1974). The Eureka Valley Tuff erupted from the Little Walker caldera (Noble et al., 1974; King et al., 2007), directly east of the Sierran crest near Sonora Pass, California (Fig. 3), and Stanislaus Group lavas erupted from the Sierra Crest graben-vent system, which covers an area of >250 km$^2$, from south of Sonora Pass and the Little Walker caldera northward nearly to Ebbetts Pass, and west from that along the modern range front (see red stars in fig. 15A of Busby et al., 2013a). The Table Mountain Formation consists of at least 23 individual latite lava flows >400 m thick in the vicinity of Sonora Peak, thinning westward to a single, 48-m-thick, paleo-canyon-filling flow terminating near Knights Ferry, bracketed in age by a 10.41 ± 0.08 Ma basal flow, and the 10.36 ± 0.06 Ma uppermost flow (top eroded) at the Sonora Peak locality (Busby et al., 2008; Gorny et al., 2009; Pluhar et al., 2009). However, the Table Mountain Formation may cover a larger time span, as there are numerous other vents besides the one at Sonora Peak (see fig. 15 of Busby et al., 2013a). Three ignimbrite members and two lava flow members compose the Eureka Valley Tuff at the type section near Sonora Pass area (Noble et al., 1974; Priest, 1979; Koerner et al., 2009; Farner et al., 2012; Fig. 4). The Tollhouse Flat Member directly overlies the Table Mountain Formation series of lavas in most regions and is the oldest ignimbrite of the Eureka Valley Tuff, although there is evidence for an earlier informal Basal Lava Flow member of the Eureka Valley Tuff at the Stanislaus Group type section (Fig. 4; Farner et al., 2012; Busby et al., 2013a). The Tollhouse Flat Member erupted ca. 9.5 Ma (Busby et al., 2008, 2013a; Pluhar et al., 2009; John et al., 2012; Fredrickson et al., 2013). Its main distinguishing characteristics from other Eureka Valley Tuff members are the presence of 1–2 mm biotite phenocrysts within pumice fragments and a reversed paleomagnetic polarity (Al Rawi, 1969; Noble et al., 1974; King et al., 2007; Pluhar et al., 2009). At least two intercalated trachyandesite to trachydacite lavas that form the Lava Flow member are found between the Tollhouse Flat and By-Day Members in and around the vicinity of the Little Walker caldera and Stanislaus Group type locality (Fig. 4; Priest, 1979; Brem, 1984; Pluhar et al., 2009; Koerner et al., 2009). Upsection is the By-Day Member, which displays normal paleomagnetic polarity and, other than xenocrystic biotites from country rock, contains no macroscopic biotite phenocrysts (Al Rawi, 1969; Noble et al., 1974; King et al., 2007; Pluhar et al., 2009). The By-Day Member has been dated as 9.42 ± 0.04 Ma (Pluhar et al., 2009). Typically less welded and less regionally distributed than the other two ignimbrite members, the Upper member is the youngest ignimbrite of the Eureka Valley Tuff ca. 9.4 Ma (Busby et al., 2008; Pluhar et al., 2009; Busby et al., 2013a). The Upper member displays a normal paleomagnetic polarity and a reoccurrence of the biotite phenocrysts seen in the Tollhouse Flat Member (Al Rawi, 1969; Noble et al., 1974; King et al., 2007; Pluhar et al., 2009). First named for outcrops in the proximity of the Dardanelle Cone, the Dardanelles Formation comprises the uppermost lavas of the Stanislaus Group (Ransome, 1898; Noble et al., 1974), which are dated as ca. 9.1 Ma (Farner et al., 2012).

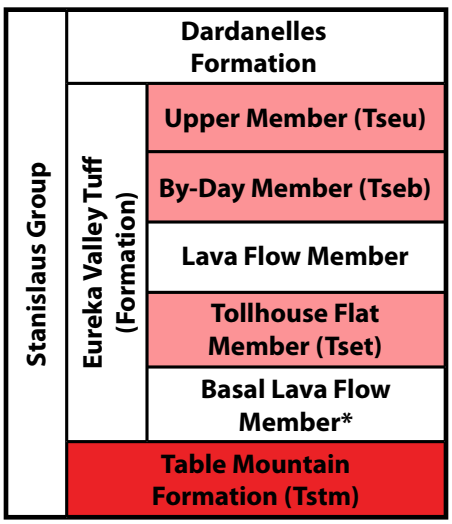


**Figure 4. Stanislaus Group nomenclature (Busby et al., 2013a). Red—Table Mountain Formation; pink—Eureka Valley Tuff members; see Figure 2 for distributions. (Asterisk indicates nomenclature from Farner et al., 2012.)**

### Walker Lane Tectonics

Various methods have been applied to understand the tectonic evolution and crustal structures within the Walker Lane. Stewart (1988) first recognized variation in styles of deformation, and implemented the use of structural blocks to subdivide the Walker Lane. These nine structural blocks were characterized by fault patterns, displacements, and apparent kinematic independence from adjacent regions (Stewart, 1988). Similar to the structural blocks of Stewart (1988), others have examined fault characteristics of the Walker Lane to differentiate the northern, central, and southern regions (e.g., Wesnousky, 2005; Faulds and Henry, 2008). Studies of active faulting within the Walker Lane show a general south to north younging in fault activation ages, resulting in better developed fault systems in the south (i.e., greater fault lengths and longer slip histories; e.g., Wesnousky, 2005; Faulds and Henry, 2008). Geodetic work in the Walker Lane has examined velocities of crustal blocks obtained with global positioning system (GPS) to define kinematic boundaries of shear for the Walker Lane. These regional studies have characterized the Walker Lane as an ~100-km-wide zone between ~40°N and 37°N, accommodating ~10 mm/yr of predominantly transtensional deformation (e.g., Bennett et al., 2003; Kreemer et al., 2009). Utilizing these velocity data, studies have also constrained domains of nonplane versus plane strain to differentiate kinematic styles of transtension and extension in the Walker Lane and adjacent regions (Oldow, 2003; Oldow et al., 2008; Murphy et al., 2009). Most recently, geodetics have been used to model vertical-axis rotations in the northern Walker Lane with present-day rates approaching 1°–2° m.y.$^{-1}$ (Hammond et al., 2011).

Paleomagnetic analyses of igneous lithologies have proven useful in constraining tectonic vertical-axis rotation and dextral shear accommodation in the Walker Lane. Cashman and Fontaine (2000) sampled regional volcanics to paleomagnetically determine vertical-axis rotation magnitudes and rates within portions of the northern Walker Lane. Their goal was to determine how dextral shear was being accommodated in portions of these domains where dextral faulting was nonexistent compared to regions in the north and south (e.g., Honey Lake–Warm Valley Springs–Pyramid Lake faults and Gumdrop Hills–Benton Springs–Petrified Springs faults, respectively). Lewis et al. (2007) utilized paleomagnetic directions from late Pliocene volcanics (determined by Pluhar et al., 2006) to support other geological and geophysical data defining regional dextral shear of the southern Walker Lane. Paleomagnetic work of Petronis et al. (2002, 2007, 2009) constrained rotations of ~20°–30° within the central Walker Lane, and the data were used by Oldow et al. (2008) to examine the evolution of the structural stepover linking the dextral faults of the southern and central Walker Lane via the Mina deflection. Similarly, King et al. (2007) and Rood et al. (2011) utilized members of the Eureka Valley Tuff to determine vertical-axis rotations with magnitudes ~25°–30° in the Anchorite Hills and Bodie Hills northwest of the Mina deflection.

## METHODS

The following provides details on collection of paleomagnetic and structural data used to establish characteristic remanent magnetization (ChRM) of lithologies from study localities. Then we describe the manner in which structurally corrected ChRM directions are compared to paleomagnetic reference directions for determining magnitudes of vertical-axis rotation of crustal blocks. We provide a brief description of the criteria for grouping rotational data into inferred domains of mean rotational magnitude as part of this study.

### Paleomagnetic Sampling

We collected 301 oriented core samples for paleomagnetic analysis from outcrops of the Eureka Valley Tuff, Table Mountain Formation, and, where they were found in a stratigraphic section with these other units, trachyandesites of Masonic Mountain and Potato Peak (John et al., 2012). At each sampled site a minimum of 7 samples, separated ≥3 m from each other across outcrop, were cored utilizing a gas-powered portable rock drill and ~2.54 cm inner diameter diamond-tipped core bit. In situ core orientations were determined using an orienting fixture to collect both magnetic and sun compass data. Sun compass corrections provided site magnetic azimuth corrections accounting for local magnetic anomalies due to lightning strikes and strongly magnetized outcrops. In addition, three oriented hand samples used in this study were collected from the Murphy Flat Overlook locality. Demagnetization experiments were performed in the Rock- and Paleo-magnetism Laboratory at the U.S. Geological Survey in Menlo Park (California). Housed in a shielded room reducing ambient magnetic field to 1% of its normal value, the multispecimen fully automated cryogenic magnetometer (Kirschvink et al., 2008) performed progressive 10-step alternating field (AF) demagnetization of specimens (0 mT [NRM, natural remanent magnetization], 2, 5, 10, 15, 20, 30, 40, 60, 80 mT). Two sampled units were further demagnetized (100, 120, 150, 180 mT) in a shielded single-axis 2G AF demagnetizer at the California State University, Fresno, Paleomagnetism Laboratory and measured on an AGICO JR6 spinner magnetometer (localities TFR04 and PLY02; Table 1). Standard least-squares and great circle analysis of specimen demagnetization data yielded ChRMs for each sample (Kirschvink, 1980; Cogné, 2003). Great circle analyses were performed on a small minority of specimens that did not converge on stable ChRMs, typically due to lightning strikes (Kirschvink, 1980; Cogné, 2003). Site mean directions for each lava flow or ignimbrite at a given site were calculated from the specimen ChRMs (and great circles when present), assuming a Fisher distribution (Fisher, 1953; McFadden and McElhinny, 1988; Cogné, 2003).

### Structural Corrections

To reliably quantify vertical-axis rotation of tectonic blocks, site mean directions had to be structurally corrected to account for tilting of the beds from their inferred paleohorizontal orientation. Tilt-corrected results were then compared to reference directions for the same unit derived from a relatively unrotated tectonic domain, such as the Sierra Nevada microplate (Demarest, 1983). When tilt corrections yielded expected paleomagnetic inclinations within $\alpha_{95}$ error, these results were deemed to be acceptable quality (Demarest, 1983). Those results that did not meet this criterion were either rejected from further consideration, or if less than a few degrees outside of acceptance (i.e., $\alpha_{95}$ error), the data were utilized but treated with extreme caution. Any declination anomalies present in the tilt-corrected paleomagnetic data were interpreted to be the result of vertical-axis rotation. Vertical-axis rotation and tilting (i.e., horizontal-axis rotation) may have occurred simultaneously via oblique-slip motion, and/or during multiple stages of deformation on various accommodating structures. Multistage deformation could introduce uncertainty into the interpretation of the tilt and rotation data. However, as tilt corrections used for the study sites were typically <30°, the level of uncertainty on the resultant vertical-axis rotations is considered negligible. This study employed ~240 structural orientation measurements for restoration of sample sites into paleohorizontal.

The principal paleohorizontal proxy for the study rocks consisted of eutaxitic textures, or compaction foliation, within the ignimbrites. This texture results from gravitational compaction of hot vitrified pumice fragments after deposition of tuffs, producing ellipsoidal flattened features, or fiamme, with the short axis oriented parallel to the maximum principal stress direction at time of formation (Chapin and Lowell, 1979; Hagstrum and Gans, 1989; McIntosh, 1991; Cashman and Fontaine, 2000; Henry et al., 2003; King et al., 2007; Pluhar et al., 2009). Structural corrections were determined by best-fit great circles to the trend and plunge of fiamme apparent dips measured in outcrops. At least 10 measurements of fiamme apparent dips were collected across outcrops at distances equivalent to sampled cores for great circle determinations. Localized perturbation of fiamme orientations due to the presence of solid state objects at the time of deposition has proven to be problematic in the use of eutaxitic textures (Chapin and Lowell, 1979; Hagstrum and Gans, 1989; McIntosh, 1991; Henry et al., 2003; King et al., 2007). Significant paleotopography in basal contact with ignimbrites has been shown to modify foliation indicators by as much as 70° from horizontal during emplacement (Henry et al., 2003). Use of foliation fabrics for sampled unit restoration to paleohorizontal required site by site evaluation for accuracy using the expected inclination criterion.

### Vertical-Axis Rotations and Domain Boundaries

Tilt-corrected mean paleomagnetic directions for sampled sites were compared to the reference directions of King et al. (2007) using the method of Demarest (1983). The Sierra Nevada microplate can be considered tectonically stable compared to the Walker Lane with respect to vertical-axis rotation and tilt during the Neogene. As a result, reference directions for members of the Eureka Valley Tuff deposited on the stable Sierra provide a measure of relative rotation of the sampled region compared to the reference region since the time of member emplacement. Statistically significant declination anomalies of a sampled unit compared to reference directions derived from the stable Sierra Nevada revealed relative vertical-axis tectonic rotations. In our analysis, we also included or reinterpreted paleomagnetic directions for sampling localities located east of the Sierran crest (nine from King et al., 2007; five from Pluhar et al., 2009).

Sampling locality vertical-axis rotations that displayed similar magnitudes were grouped together to establish rotational domains. Our rotational domains represent a region within which multiple tectonic blocks have accommodated similar magnitudes of vertical-axis rotation, rather than the cohesive rotation of one region of fault-bound crust. Once groups of similar rotation magnitude had been defined, geologic (e.g., Al Rawi, 1969; Priest, 1979; Brem, 1984; John et al., 2012; Busby et al., 2013b) and Quaternary active faulting maps (U.S. Geological Survey Earthquake Hazards Program, 2006) were consulted to identify domain boundary structures that would potentially accommodate differential rotation between adjacent domains. When mapped faults were not present between regions of different rotation magnitude, the use of geomorphic features (e.g., linear drainages, breaks in slope, aligned depositional basins) indicative of faulting aided in positioning of domain boundaries. This was an important consideration, because vertical-axis rotation may

TABLE 1. PALEOMAGNETIC RESULTS

| Location name<br>Sample site identification | Sample lithology | n | Declination (geog.) (°) | Inclination (geog.) (°) | Declination (strat.) (°) | Inclination (strat.) (°) | *k* | $\alpha_{95}$ | ChRM type | Strike (°) | Dip (°) | Latitude (NAD83) | Longitude (NAD83) |
|---|---|---|---|---|---|---|---|---|---|---|---|---|---|
| Aurora Peak (west of) | | | | | | | | | | | | | |
| APW01 | unknown tuff (Tset?) | 6 | 280.3 | –31.7 | 294.3 | –26.5 | 202.4 | 4.7 | Fisher | 96 | 25SW | N38.26359 | W118.87807 |
| Atastra Creek | | | | | | | | | | | | | |
| ATC01 | Tset | 7 | 205.2 | –62.7 | 211.8 | –57 | 555 | 2.6 | Fisher | 333 | 7NE | N38.25333 | W118.98640 |
| ATC02 | Tseu | 8 | 12 | 32.8 | 15.1 | 28.4 | 248.5 | 3.5 | Fisher | 333 | 7NE | N38.25390 | W118.98720 |
| ATC03 | Tseu | 5 | 14.4 | 33.1 | 17.4 | 28.4 | 708.9 | 2.9 | Fisher | 333 | 7NE | N38.25380 | W118.98736 |
| ATC04 | Tseu | 6 | 17.3 | 38.1 | 20.7 | 33.2 | 189.3 | 4.9 | Fisher | 333 | 7NE | N38.25375 | W118.98765 |
| ATC05* | Potato Peak Dacite | 4 | 111.1 | 72.6 | 98.5 | 67.5 | 115.9 | 8.6 | Fisher | 333 | 7NE | N38.25470 | W118.98840 |
| Boone Canyon | | | | | | | | | | | | | |
| BOC02 | Tseb | 6 | 50.2 | 44.8 | 24.9 | 50.7 | 188.8 | 4.9 | Fisher | 203 | 23NW | N38.34446 | W119.25050 |
| BOC03 | Tseb | 6 | 47 | 37.5 | 26.8 | 48.2 | 219.8 | 4.5 | Fisher | 191 | 24NW | N38.34464 | W119.24907 |
| BOC04 | Tset | 7 | 233.5 | –40.9 | 211 | –53.6 | 506.6 | 2.9 | mixed | 191 | 24NW | N38.34373 | W119.24799 |
| BOC05 | Tstm (?) | 8 | 246.4 | –36.2 | 229.8 | –54 | 95.2 | 5.7 | Fisher | 191 | 24NW | N38.34279 | W119.24837 |
| Chemung Mine | | | | | | | | | | | | | |
| CHE01 | Tset | 7 | 167.5 | –53.3 | 160.4 | –64.2 | 431.4 | 2.9 | Fisher | 96 | 12SW | N38.35190 | W119.15550 |
| CHE02* | Masonic Andesite | 8 | 18.3 | 37.7 | 20.5 | 30.1 | 130.9 | 5.1 | mixed | 313 | 8NE | N38.34848 | W119.15907 |
| CHE03* | unknown lava | 7 | 25 | 16.8 | 25.5 | 8.9 | 12.9 | 18.5 | mixed | 313 | 8NE | N38.34880 | W119.15910 |
| CHE04* | unknown lava | 8 | 234.2 | 0.2 | 234.2 | 8.4 | 175.2 | 4.4 | Fisher | 312 | 8NE | N38.34943 | W119.16032 |
| CHE06 | Tset | 7 | 183.5 | –48 | 188.4 | –41.4 | 316.5 | 3.4 | mixed | 313 | 8NE | N38.34971 | W119.16052 |
| CHE07* | unknown lava | 5 | 344.9 | 29.7 | 342.8 | 21.9 | 11.3 | 25.1 | mixed | 225 | 9NW | N38.35166 | W119.15447 |
| Cloudburst Creek | | | | | | | | | | | | | |
| CLB17† | Tstm | 9 | 336.6 | 47.9 | 338.9 | 23 | 537.3 | 2.2 | Fisher | 255 | 25NW | N38.35652 | W119.56967 |
| CLB18† | Tstm | 9 | 9.5 | 75.6 | 354.6 | 51.3 | 181.1 | 3.9 | mixed | 255 | 25NW | N38.35683 | W119.57004 |
| CLB19† | Tstm | 9 | 315.3 | 51.1 | 324.4 | 28.3 | 26.8 | 10.4 | mixed | 255 | 25NW | N38.35711 | W119.57091 |
| East Walker River (east side) | | | | | | | | | | | | | |
| EWE01 | Tset | 9 | 235.4 | –62.7 | 219.9 | –56.4 | 59.4 | 6.7 | Fisher | 262 | 11NW | N38.34532 | W119.20626 |
| Halfway Cabin | | | | | | | | | | | | | |
| HWC01 | Tset | 9 | 149.1 | –42.7 | 194.5 | –58 | 27.6 | 10.7 | Fisher | 13 | 38SE | N38.29960 | W119.05210 |
| HWC02* | unknown lava | 6 | 183.3 | –62.7 | 160.5 | –50.3 | 289.8 | 3.9 | Fisher | 211 | 19NW | N38.30185 | W119.05170 |
| HWC03* | unknown lava | 9 | 180.8 | –54.3 | 163.8 | –42.1 | 26.2 | 11 | mixed | 211 | 19NW | N38.30202 | W119.05250 |
| HWC04* | unknown lava | 8 | 358.4 | 30.7 | 351.1 | 19.2 | 91.8 | 6.1 | mixed | 211 | 19NW | N38.30238 | W119.05330 |
| Homestead Mine | | | | | | | | | | | | | |
| HM01 | Tset | 10 | 191.2 | –61.7 | 182.8 | –59.9 | 143.9 | 4.6 | Fisher | 208 | 5NW | N38.37235 | W119.00068 |
| Murphy Flat Overlook | | | | | | | | | | | | | |
| MFO | Tseu | 3 | 22.8 | 44.3 | 0.9 | 31.9 | 285.7 | 7.3 | Fisher | 216 | 30NW | N38.36862 | W119.269531 |
| McMillan (Spring) Creek | | | | | | | | | | | | | |
| MMC01 | Tset | 10 | 49.5 | 41.2 | 29.9 | 26.6 | 242.3 | 3.2 | mixed | 246 | 32NW | N38.31906 | W119.18922 |
| Murphy Spring | | | | | | | | | | | | | |
| MSP01 | Tset | 11 | 294 | –65.4 | 227.3 | –78.3 | 634 | 1.8 | Fisher | 233 | 23NW | N38.18407 | W119.06795 |
| Playa (near Atastra Creek) | | | | | | | | | | | | | |
| PLY02 | Tseb | 9 | 358.3 | 56.5 | 5.9 | 43.8 | 66.8 | 6.4 | mixed | 299 | 14NE | N38.27581 | W119.01010 |
| PLY03* | unknown tuff | 8 | 15.8 | –70.7 | 347.2 | –83.7 | 35.9 | 9.6 | mixed | 299 | 14NE | N38.27496 | W119.01099 |
| Red Rock Creek | | | | | | | | | | | | | |
| RRC01 | Tset | 10 | 194.7 | –55.8 | 169.7 | –61.1 | 490.3 | 2.2 | Fisher | 164 | 16SW | N38.43458 | W119.08424 |
| Rock Springs Canyon | | | | | | | | | | | | | |
| RSC01 | Tset | 11 | 218.9 | –45.1 | 183.7 | –60.7 | 289.7 | 2.7 | mixed | 172 | 30SW | N38.28716 | W119.14586 |
| Tollhouse Flat (reference section) | | | | | | | | | | | | | |
| TFR01† | Tstm (?) | 7 | 271.1 | 77.9 | 11.3 | 64.9 | 73.2 | 7.1 | Fisher | 305 | 30NE | N38.42699 | W119.44785 |
| TFR02 | Tset | 8 | 14.4 | –82.5 | 201.6 | –62.9 | 453.9 | 2.6 | Fisher | 290 | 35NE | N38.42779 | W119.44875 |
| TFR03 | Tseb | 9 | 36.3 | 84.5 | 24.5 | 53 | 449.2 | 2.4 | Fisher | 292 | 32NE | N38.42942 | W119.44910 |
| TFR04† | Tseu | 3 | 328.3 | 73.5 | 353.5 | 44.6 | 82.6 | 13.7 | Fisher | 278 | 32NE | N38.42997 | W119.44823 |

*Note:* Sample lithology abbreviations as in Figure 4. NAD—North American Datum; geog.—geographic; strat.—stratigraphic; *k*—precision parameter; ChRM—characteristic remanent magnetization.
*Non-Stanislaus Group lithologies not used as part of study.
†Stanislaus Group lithologies that provided insufficient data for use in study.

not be currently occurring in the region and older tectonic structures (e.g., strike-slip faults) are obscured by younger stratigraphy.

## RESULTS

We describe behavior and statistics of paleomagnetic data used in this study at the site and locality level. For stratigraphic sections with multiple Eureka Valley Tuff members, we address differences in rotation magnitudes evident between different members for the same locality, leading to revisions of previously published paleomagnetic reference directions and identification of regions of previously unrecognized vertical-axis crustal block rotation. We then present vertical-axis rotation magnitudes determined by comparison of site paleomagnetic directions to reference directions previously published (Tollhouse Flat Member) or revised as part of this study (By Day Member and Upper member).

### Paleomagnetic Directions

Alternating-field demagnetization experiments revealed ChRMs for the majority of paleomagnetic samples collected in this study. Upon removal of minor secondary magnetization components, sample specimens typically produced univectorial demagnetization paths toward the origin defined by four or more steps (Fig. 5). These sample ChRMs usually exhibited maximum angular deviations of <1° for any given specimen. Removal of secondary magnetization components (or magnetic overprints) from most of the study samples was accomplished by 10 mT or 15 mT, with the median destructive fields typically ~20 mT for lavas, and 60 mT for ignimbrites (Fig. 5). Rock magnetic experiments were not performed as part of this study, but previous work identified titanomagnetite for ignimbritic lithologies of the Eureka Valley Tuff (King et al., 2007; Rood et al., 2011), and both titanomagnetite and titanohematite in flows from the Table Mountain Formation (King et al., 2007). The high mean destructive field of ignimbrite samples is suggestive of single-domain or pseudosingle-domain magnetic minerals within these lithologies. Easy removal of secondary magnetization and the presence of probable original magnetic carrier mineralogy make these rocks ideal for paleomagnetic study.

Mean ChRMs for each sampled unit were typically derived from 6 or more independent samples, and yielded Fisher statistics of $\alpha_{95}$ < 10.0° (arithmetic mean for study was 5.9°) and $k$ of > 60 (arithmetic mean for study was 272) (Table 1). The one exception to angular deviation <10° still used for the purpose of vertical-axis rotational analysis was the Tollhouse Flat Member at the Halfway Cabin locality (Table 1). This locality was deemed useful because the angular dispersion was only slightly higher, 10.7°, and was in close proximity to other localities displaying similar statistically significant rotations. Sample ChRMs were combined with great-circle analysis for 5 of 20 sites sampled in this study used to determine magnitudes of vertical-axis rotation (Table 1). In most cases sample paleomagnetic directions for the Eureka Valley Tuff exhibited expected polarities (Al Rawi, 1969; Noble et al., 1974; King et al., 2007; Pluhar et al., 2009). Otherwise, the paleomagnetic results were used to correct the mapped or infield ignimbrite identifications. For example, several highly welded sites at Atastra Creek originally thought to be the By-Day Member were later determined to be the Upper member. Table Mountain Formation lavas at two sampled localities were positioned stratigraphically below and in basal contact with the Tollhouse Flat Member (Brem, 1984; King et al., 2007; Table 1). The ChRM for the lava at the Tollhouse Flat Reference Section locality produced a normal paleomagnetic polarity, whereas the Boone Canyon lava was reversed (Table 1). The reversed polarity of the Boone Canyon lava was of particular interest because nearly all Table Mountain Formation flows studied so far exhibit normal polarity (e.g., Pluhar et al., 2009), although there are extensive areas of the Table Mountain Formation that have not been studied paleomagnetically. The Boone Canyon lava mean ChRM may correspond in terms of inclination to (1) the Table Mountain flow 19 at Sonora Peak, erupted during the Sonora Peak event magnetic excursion (Pluhar et al., 2009); (2) flow 5 at Patterson Canyon on the southeast margin of the Little Walker caldera (Pluhar et al., 2009); and/or Table Mountain Formation lavas found near Hetch Hetchy, California (Huber, 1990; Jones et al., 2013). The fact that the Boone Canyon locality underwent tens of degrees of vertical axis rotation (see following) makes a correlation of the Boone Canyon lava uncertain based solely on paleomagnetic direction. Because these sites may represent a regionally extensive lava useful for follow-up tectonic studies, future geochemical work will be needed to test these potential paleomagnetic correlations.

### Revised Reference Directions

Comparison of mean site ChRMs for Eureka Valley Tuff members in the study area to published reference directions of King et al. (2007) revealed a problem. Three localities east of the Sierran crest exhibit more than one member of the Eureka Valley Tuff, in stratigraphic section, and rotation calculations using the published reference directions for these sites yielded statistically significant differences between measured rotations for each member (Table 2). These differences in sample site rotations at the same locality could result from two possible scenarios: (1) extremely high tectonic activity with measurable rotation occurring between emplacement of the Eureka Valley Tuff members (i.e., interdepositional rotation, analogous to growth faulting horizontal-axis rotation), or (2) inaccurate reference directions for the Eureka Valley Tuff members because the By-Day Member and Upper member reference sites were located in regions that underwent significant vertical-axis rotation. A notable problem for the interdepositional tectonics hypothesis (case 1) is that the vertical-axis rotation of localities in question would require extreme interdepositional rotation rates constrained to a minimum of ~70° m.y.$^{-1}$, based on maximum differences in unit ages and minimum statistical difference in site rotations (Table 2). At such rates, all of the measured rotation on the studied rocks would have occurred by the latest Miocene. In addition, such exceedingly high rotation rates are unrealistic over such a broad region. Because reference directions for the By-Day Member and Upper member were derived from localities east of the Sierran crest and major faults of the frontal fault system (see Busby et al., 2008, 2013a), a more likely explanation is that the reference direction sample sites of King et al. (2007) underwent previously unrecognized vertical-axis rotations (as corroborated in Farner et al., 2012). We propose new reference directions for By-Day Member and Upper member of the Eureka Valley Tuff, obviating the necessity for interdepositional tectonics, although our results still permit as much as ~10° of interdepositional rotation within error of measurements (e.g., Boone Canyon and Tollhouse Flat reference sections) (Table 3).

We used sampled localities (from Pluhar et al., 2009) to calculate an indirect correction of the By-Day reference direction. The Grouse Meadow locality (Pluhar et al., 2009) was selected to independently test for unrecognized rotation of By-Day Member reference direction sites of King et al. (2007). The Grouse Meadow locality consists of 16 lavas of the Table Mountain Formation capped by the By-Day Member (Busby et al., 2008, 2013b; Pluhar et al., 2009). This presented an opportunity to compare the Grouse Meadow mean paleomagnetic direction of these 16 lavas to the mean direction of 23 Table Mountain Formation lavas present at Sonora Peak (Pluhar et al., 2009). Recent

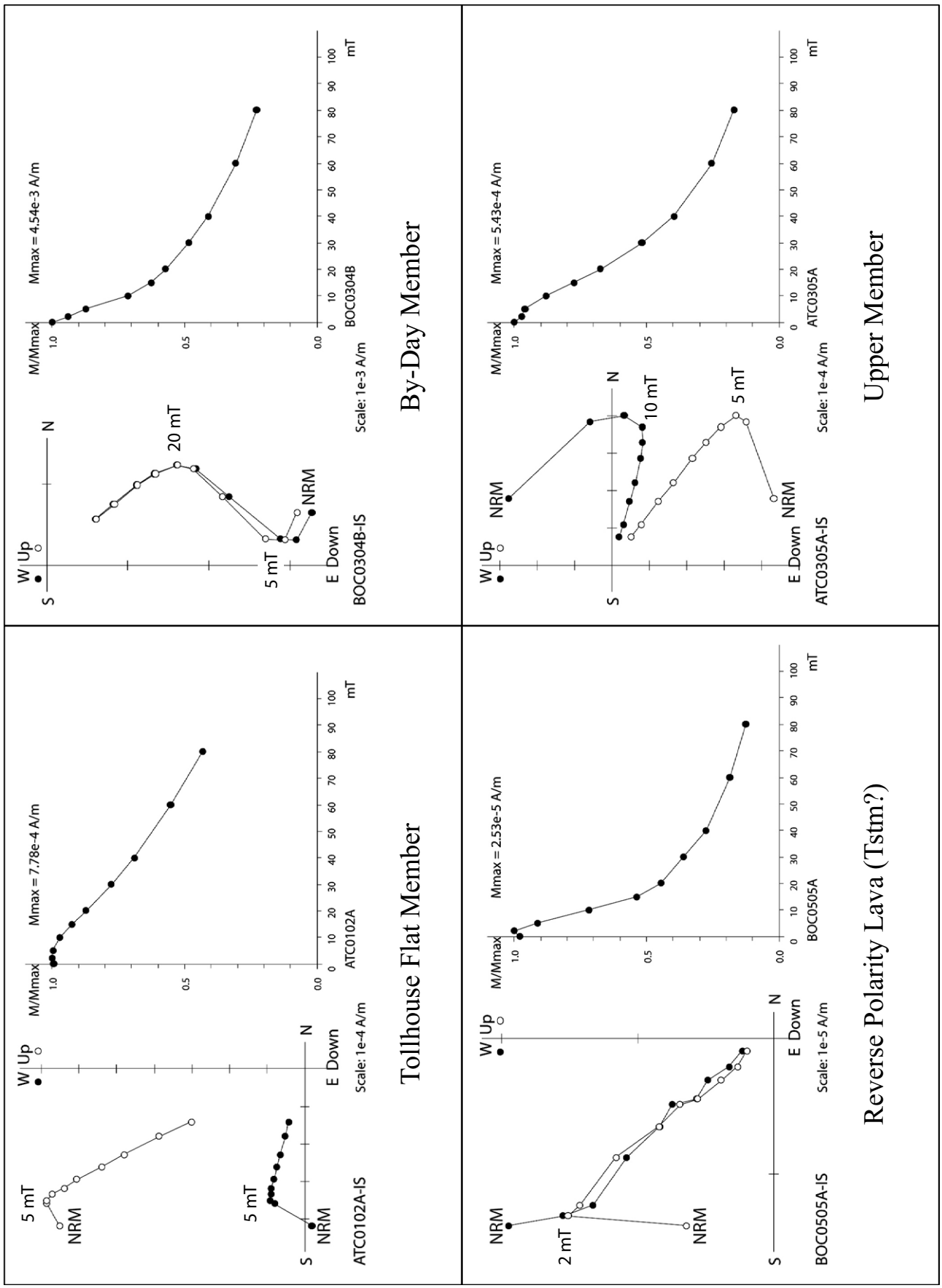


**Figure 5. Zijderveld (1967) diagrams representing progressive stepwise demagnetization experiments on Stanislaus Group specimens (sample identifications at lower left). Samples display removal of secondary components followed by univectorial decay toward the origin. See text for complete list of demagnetization steps. NRM—natural remanent magnetization.**

TABLE 2. SAMPLE LOCALITY ROTATION AND AGE VARIATIONS

| Sample locality name | Site identifications | Unit | Unit age (Ma) | Rotation* (°) |
|---|---|---|---|---|
| Tollhouse Flat (reference section) | TFR03 | Tseb | 9.42 ± 0.03 | 15.9 ±10.0 |
| Tollhouse Flat (reference section) | TFR02 | Tset | ca. 9.5 | 44.7 ± 6.8 |
| Boone Canyon | BOC03, BOC02 | Tseb | 9.42 ± 0.03 | 17.9 ± 10.2 |
| Boone Canyon | BOC04 | Tset | ca. 9.5 | 48.7 ± 6.1 |
| Atastra Creek | ATC02, ATC03, ATC04 | Tseu | ca. 9.4 | 19.8 ± 9.8 |
| Atastra Creek | ATC01 | Tset | ca. 9.5 | 42.8 ± 6.0 |

*Note:* Reference directions used to calculate rotation are from King et al. (2007). Unit labels (see Fig. 4): Tset—Tollhouse Flat Member of the Eureka Valley Tuff (EVT); Tseb—By-Day Member of EVT; Tseu—Upper member of EVT.

*Calculated using method of Demarest (1983).

detailed mapping of the Sierra Crest graben-vent system has identified components of dextral and sinistral slip on normal faults in the Sonora Peak region active since ca. 12 Ma, and interpreted to be the time of formation of the Sierra Nevada microplate (Busby, 2013; Busby et al., 2013b). While these oblique slips may have accommodated vertical-axis rotation, the present-day mean paleomagnetic direction of the Sonora Peak lavas is statistically indistinguishable from the Miocene reference pole for North America (Hillhouse and Grommé, 2011). Therefore we consider the Sonora Peak locality a relatively stable platform for paleomagnetic comparison to Grouse Meadow to the east.

Mean paleomagnetic directions of Sonora Peak and Grouse Meadow Table Mountain Formation lavas are statistically indistinguishable in inclination (flattening = 0.5° ± 5.3°), but yield a declination anomaly of 18.7° ± 8.8° clockwise for the Grouse Meadow locality (Table 3; Fig. 6). This difference in declination was used to back rotate counterclockwise the Grouse Meadow locality into a stable Sierra Nevada reference frame. This provides a recalculated reference direction for the By-Day Member of declination (dec.) = 353.2°; inclination (inc.) = 43.7°, $\alpha_{95}$ = 10.8°. The North American Miocene reference pole of Hagstrum et al. (1987) provided an additional source for rotational comparison of Grouse Meadow independent of Sonora Peak. In this case the virtual geomagnetic pole calculated for Grouse Meadow lavas (lat 77.8°, long 349.6°, $\alpha_{95}$ = 6.5°) exhibits a declination anomaly relative to the published Miocene reference pole (lat 87.4°, long 129.7°; $\alpha_{95}$ = 3.0°) and implies a clockwise rotation of 15.6° ± 7.5° for Grouse Meadow. Both methods of calculating rotation for Grouse Meadow support the revision of the published reference direction for the By-Day Member (King et al., 2007). The Eureka Valley Tuff at the Stanislaus Group type section was sampled (by Farner et al., 2012), producing a mean ChRM direction from the relatively stable Sierra Nevada

TABLE 3. SAMPLE SITE ROTATION CALCULATIONS

| Sample locality name (this study) | Sampled site identification | Unit | Declination (tilt corrected, °) | Inclination (tilt corrected, °) | Unit $\alpha_{95}$ (°) | Reference declination (°) | Reference inclination (°) | Reference $\alpha_{95}$ (°) | Flattening* (°) | Rotation† (°) |
|---|---|---|---|---|---|---|---|---|---|---|
| Tollhouse Flat (reference section) | TFR | Tseb | 24.5 | 53.0 | 2.4 | 349.6 | 51.9 | 3.0 | 1.1 ± 3.1 | 34.9 ± 5.0 |
| Tollhouse Flat (reference section) | TFR | Tset | 204.6 | –65.8 | 2.6 | 159.9 | –62.8 | 2.6 | –3.0 ± 2.9 | 44.7 ± 6.8 |
| Murphy Flat Overlook | MFO | Tseu | 0.9 | 31.9 | 7.3 | 335.0 | 30.5 | 13.0 | 1.4 ± 7.6 | 25.9 ± 13.9 |
| Boone Canyon§ | BOC | Tseb | 26.5 | 48.6 | 3.1 | 349.6 | 51.9 | 3.0 | –3.3 ± 3.5 | 36.9 ± 5.4 |
| Boone Canyon | BOC | Tset | 208.6 | –55.1 | 2.9 | 159.9 | –62.8 | 2.6 | 7.7 ± 3.1 | 48.7 ± 6.1 |
| E. Walker River (eastside) | EWE | Tset | 219.9 | –56.4 | 6.7 | 159.9 | –62.8 | 2.6 | 6.4 ± 5.7 | 60.0 ± 10.8 |
| McMillan (Spring) Creek | MMC | Tseu | 30.2 | 26.9 | 2.9 | 335.0 | 30.5 | 13.0 | –3.6 ± 5.4 | 55.2 ± 12.4 |
| Chemung Mine | CHE | Tset | 171.6 | –62.5 | 3.7 | 159.9 | –62.8 | 2.6 | 0.3 ± 3.6 | 11.7 ± 7.9 |
| Red Rock Creek | RRC | Tset | 169.7 | –61.1 | 2.2 | 159.9 | –62.8 | 2.6 | 1.7 ± 2.7 | 9.8 ± 5.8 |
| Rock Springs Creek | RSC | Tset | 183.7 | –60.7 | 2.7 | 159.9 | –62.8 | 2.6 | 2.1 ± 3.0 | 23.8 ± 6.3 |
| Halfway Cabin | HWC | Tset | 194.5 | –58.0 | 10.7 | 159.9 | –62.8 | 2.6 | 4.8 ± 8.8 | 34.6 ± 17.0 |
| Playa (near Atastra Creek) | PLY | Tseb | 5.9 | 43.8 | 6.4 | 349.6 | 51.9 | 3.0 | –8.1 ± 5.7 | 16.3 ± 8.1 |
| Atastra Creek§ | ATC | Tseu | 17.8 | 30.5 | 2.7 | 335.0 | 30.5 | 13.0 | 0.0 ± 5.3 | 42.8 ± 12.4 |
| Atastra Creek | ATC | Tset | 202.7 | –58.2 | 2.6 | 159.9 | –62.8 | 2.6 | 4.6 ± 2.9 | 42.8 ± 6.0 |
| Homestead Mine | HM | Tset | 182.8 | –59.9 | 4.6 | 159.9 | –62.8 | 2.6 | 2.9 ± 4.2 | 22.9 ± 8.7 |
| Sample locality name (Pluhar et al., 2009) | | | | | | | | | | |
| Sonora Peak§ | SP | Tstm | 355.0 | 52.2 | 4.3 | | | | N/A | N/A |
| Grouse Meadow | GM | Tseb | 11.9 | 43.7 | 4.3 | 349.6 | 51.9 | 3.0 | –8.2 ± 4.2 | 22.3 ± 6.2 |
| Grouse Meadow§ | GM | Tstm | 13.7 | 52.7 | 5.1 | 355.0 | 52.2 | 4.3 | 0.5 ± 5.3 | 18.7 ± 8.8 |
| Burcham Creek | BC | Tseb | 359.4 | 40.3 | 4.7 | 349.6 | 51.9 | 3.0 | –11.6 ± 4.5 | 9.8 ± 6.3 |
| Burcham Creek | BC | Tset | 183.3 | –62.9 | 2.4 | 159.9 | –62.8 | 2.6 | –0.1 ± 2.8 | 23.4 ± 6.2 |
| Patterson Canyon | PC | Tseb | 5.0 | 52.6 | 2.0 | 349.6 | 51.9 | 3.0 | 0.7 ± 2.9 | 15.4 ± 4.7 |
| By-Day Canyon | BDC | Tseb | 4.4 | 41.1 | 7.7 | 349.6 | 51.9 | 3.0 | –10.8 ± 6.6 | 14.8 ± 9.1 |
| By-Day Canyon | BDC | Tset | 179.2 | –58.6 | 4.7 | 159.9 | –62.8 | 2.6 | 4.2 ± 4.3 | 19.3 ± 8.6 |
| Sample locality name (King et al., 2007) | | | | | | | | | | |
| LW23 | LW23 | Tseb | 16.5 | 48.4 | 8.5 | 349.6 | 51.9 | 3.0 | –3.5 ± 7.2 | 26.9 ± 11.0 |
| LW92 | LW92 | Tseb | 2.9 | 48.0 | 5.7 | 349.6 | 51.9 | 3.0 | –3.9 ± 5.2 | 13.3 ± 7.9 |
| LW93 | LW93 | Tseb | 9.4 | 54.0 | 4.9 | 349.6 | 51.9 | 3.0 | 2.1 ± 4.6 | 19.8 ± 7.7 |
| LW96 | LW96 | Tseu | 0.7 | 28.3 | 3.3 | 335.0 | 30.5 | 13.0 | –2.2 ± 5.5 | 25.7 ± 12.5 |
| 3V156 | 3V156 | Tseu | 355.4 | 27.5 | 3.3 | 335.0 | 30.5 | 13.0 | –3.0 ± 5.5 | 20.4 ± 12.5 |
| LW86 | LW86 | Tset | 166.5 | –62.1 | 4.4 | 159.9 | –62.8 | 2.6 | 0.7 ± 4.1 | 6.6 ± 8.8 |
| 3V138 | 3V138 | Tset | 170.6 | –63.6 | 2.6 | 159.9 | –62.8 | 2.6 | –0.8 ± 2.9 | 10.7 ± 6.5 |
| LW88 | LW88 | Tset | 182.8 | –56.2 | 6.7 | 159.9 | –62.8 | 2.6 | 6.6 ± 5.7 | 22.9 ± 10.7 |
| 3V129 | 3V129 | Tset | 186.1 | –59.9 | 4.0 | 159.9 | –62.8 | 2.6 | 2.9 ± 3.8 | 26.2 ± 7.9 |

*Note:* Unit labels: Tstm—Lavas of the Table Mountain Formation, Tset—Tollhouse Flat Member of the Eureka Valley Tuff (EVT); Tseb—By-Day Member of EVT; Tseu—Upper Member of EVT. Reference directions for Tset from King et al. (2007); reference directions for Tseb and Tseu derived as part of this study. $\alpha_{95}$ is radius of 95% confidence circle. N/A—not applicable.

*Rotation around a horizontal axis calculated by the method of Demarest (1983).

†Rotation around a vertical axis calculated by the method of Demarest (1983).

§Mean paleomagnetic direction calculated from multiple sites.

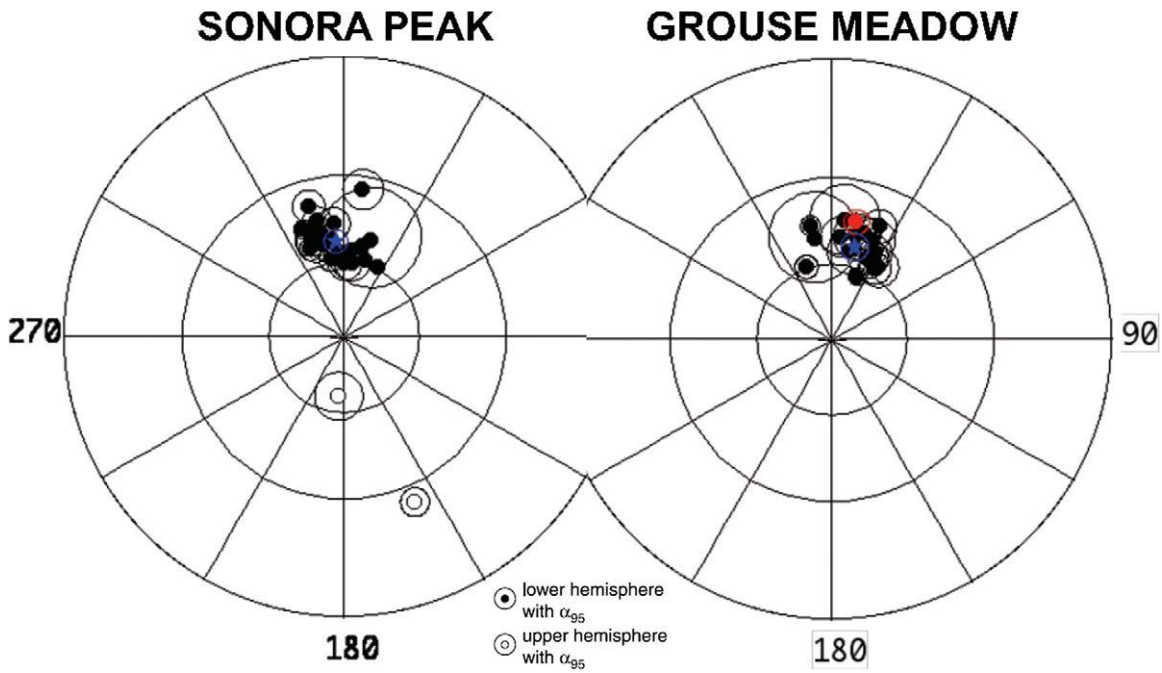


**Figure 6. Stereonets showing paleomagnetic remanence directions used to average secular variation for Sonora Peak and Grouse Meadow localities (from Pluhar et al., 2009). Mean directions for individual lava flows of the Table Mountain Formation (open or filled black circles, with $\alpha_{95}$ error radius), averaged paleomagnetic direction (blue star, with $\alpha_{95}$ error radius) of normal polarity lavas for each locality, and remanent direction of the By-Day Member at Grouse Meadow (red filled circle, with $\alpha_{95}$ error radius) are shown. The differences in averaged paleomagnetic directions (blue stars) are used in this study to back rotate the Grouse Meadow locality into a relative stable reference frame and infer a new reference direction for the By-Day Member.**

microplate for the By-Day Member: dec. = 349.6°, inc. = 52.9°, $\alpha_{95}$ = 3.0°. Their remanence direction for the By-Day Member was statistically indistinguishable in declination from that derived in this study after applying the counterclockwise back-rotation correction of virtual geomagnetic pole and site mean direction (356.3° ± 9.6° and 353.2° ± 10.8°, respectively), and statistically indistinguishable in inclination to the reference direction of King et al. (2007; By-Day Member inc. = 52.4° ± 7.2°). For these two reasons, and because they sampled from a region of the Sierra Nevada we consider to be relatively stable, we consider the remanence direction measured from the Eureka Valley Tuff type section (by Farner et al., 2012) to be the most reliable for use as the By-Day Member reference direction. Use of this recalculated reference direction eliminated any statistically significant differences in site rotations at localities where both the By-Day and Tollhouse Flat Members were present (e.g., BOC and TFR, Table 3). Thus, we have chosen the paleomagnetic direction from the type section for analysis of vertical-axis rotations where the By-Day Member was sampled in this and previous studies.

Because the previously published reference direction for the By-Day Member was determined to be derived from a rotated region, we assert that the Upper member reference direction is similarly problematic. However, the Upper member is not found at any localities where it can be independently verified using time-averaged field directions, as we have done with the By-Day Member reference direction. A mean rotational difference of ~23.0° ± 11.5° was present between the Upper member and Tollhouse Flat Member at the Atastra Creek locality (Table 2). Because no opportunities currently exist to independently check the Upper member reference direction, we assume that the 23.0° rotational difference between the Upper member and Tollhouse Flat Member directions from Atastra Creek also originates from unrecognized rotations of reference localities. Because it was considered useful for the purpose of a qualitative analysis of regional rotations, we back rotated the Atastra Creek locality direction counterclockwise 23.0° and estimated a corrected reference direction for the Upper member of dec. = 335.0°, inc. = 30.5°, $\alpha_{95}$ ~13.0°. The error is approximated because the Upper member ChRM error is propagated, in part, with itself. We tentatively used this Upper member reference direction to examine rotations of localities in the study area. To illustrate differences in calculated rotations, we use red arrows for the original reference direction of King et al. (2007) in Figure 7 and modify those same Upper member sites in Figure 8 to black arrows, and resultant larger rotations, based on our tentatively corrected reference direction.

### Vertical-Axis Rotations

Tilt-corrected mean ChRMs for the Eureka Valley Tuff members at 14 sampling localities collected in this study were compared to our newly derived paleomagnetic reference directions and that of King et al. (2007) for the Eureka Valley Tuff Tollhouse Flat Member (Table 3; Fig. 7). Three localities discussed in the following were not used for determining vertical-axis rotations (Table 1). Of the remaining 11 localities utilized to constrain rotations, 8 returned data that satisfied the criterion of replicating the ignimbrite reference inclination, permitting confident determinations of vertical-axis rotations (Table 3). Although directions at the remaining three localities did not rigorously satisfy acceptance criteria, they were broadly consistent with nearby localities (Table 3; Fig. 7). The statistically significant inclination anomalies

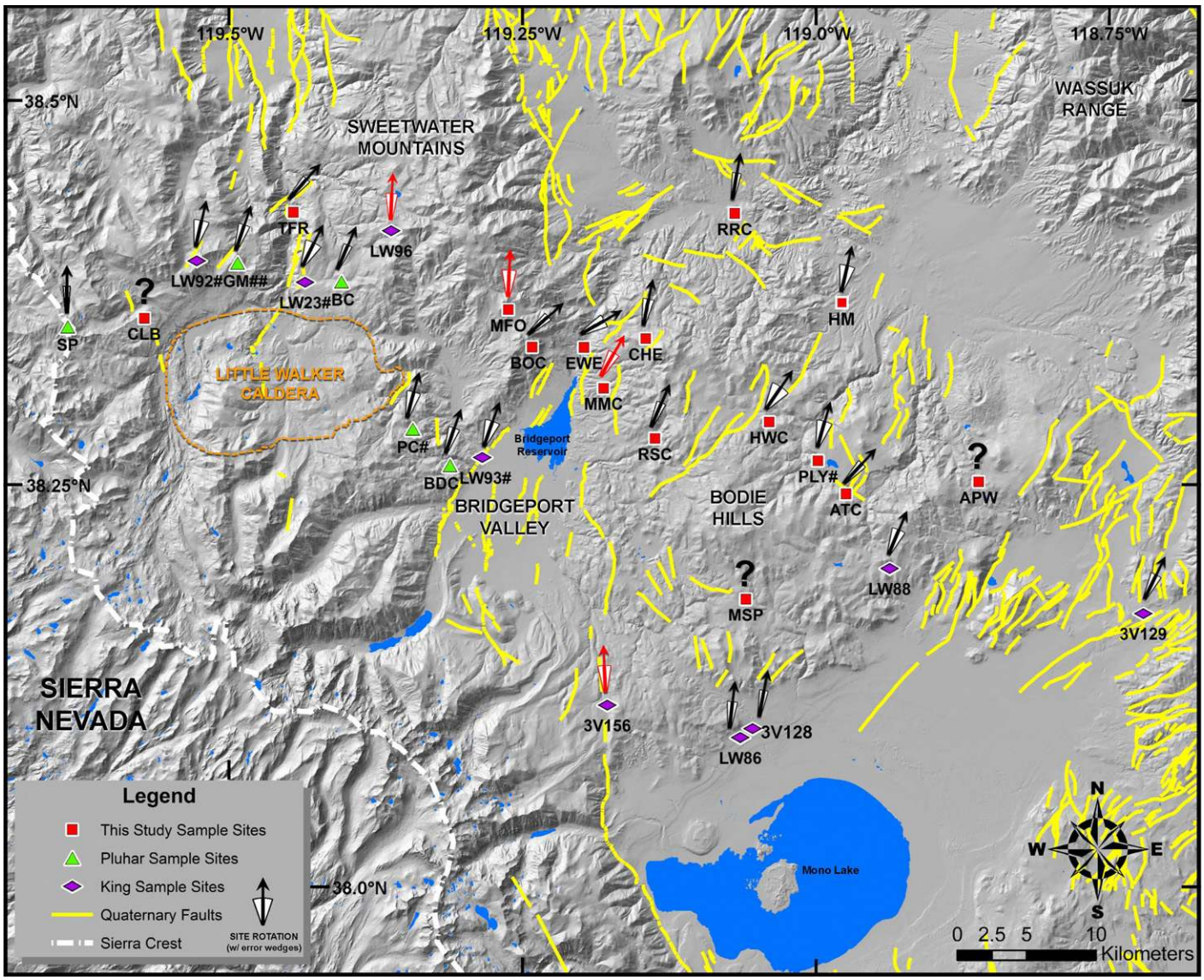


**Figure 7. Paleomagnetic sampling locality vertical-axis rotation magnitudes. Arrows (black) depict rotation magnitudes referenced from north; wedges bounding rotation arrows represent statistical error ($\alpha_{95}$), of each rotation measurement. Red arrows represent site rotations determined using the Upper member reference direction of King et al. (2007). #Site rotations determined using the By-Day Member reference direction from the Eureka Valley Tuff type section (Farner et al., 2012). ##Grouse Meadow location (GM; Pluhar et al., 2009) used to identify problematic reference directions from King et al. (2007). Queried (?) sites are those that failed to return useable paleomagnetic directions, as indicated by characteristic remanent magnetization (ChRM) inclination anomalies or insufficient averaging of secular variation. Paleomagnetic data sources: red squares—this study; green triangles—Pluhar et al. (2009); purple diamonds—King et al. (2007). See Table 1 for locality nomenclature, global positioning system coordinates (latitude and longitude), and sampled lithologies collected as part of this study. Site abbreviations as in Table 3.**

(flattening) of a few degrees for these sites is considered insignificant in this study based on the magnitudes of measured site rotations. Inclination anomalies probably resulted from original dip of eutaxitic textures due to deposition over significant paleotopography (Chapin and Lowell, 1979; Hagstrum and Gans, 1989; McIntosh, 1991). The localities Aurora Peak West and Murphy Spring returned paleomagnetic inclinations well outside the acceptance criterion of this study and were rejected from further consideration (queried locations APW and MSP in Fig. 7). The remaining unused locality, Cloudburst Creek (queried location CLB in Fig. 7), consisted of three sampled lavas that failed to adequately sample secular variation and were not correlatable to previously sampled sites elsewhere using remanence directions alone (e.g., Table Mountain Formation lava sites of Pluhar et al., 2009). Additional localities (14; from the work of King et al., 2007; Pluhar et al., 2009) were referenced or reevaluated for additional rotation data within the study region (Fig. 7; Table 3). Rotations determined in this study ranged from as little as 9.8° ± 5.8° to as much as 60.0° ± 10.8° across the study region east of the Sierran crest (Table 3).

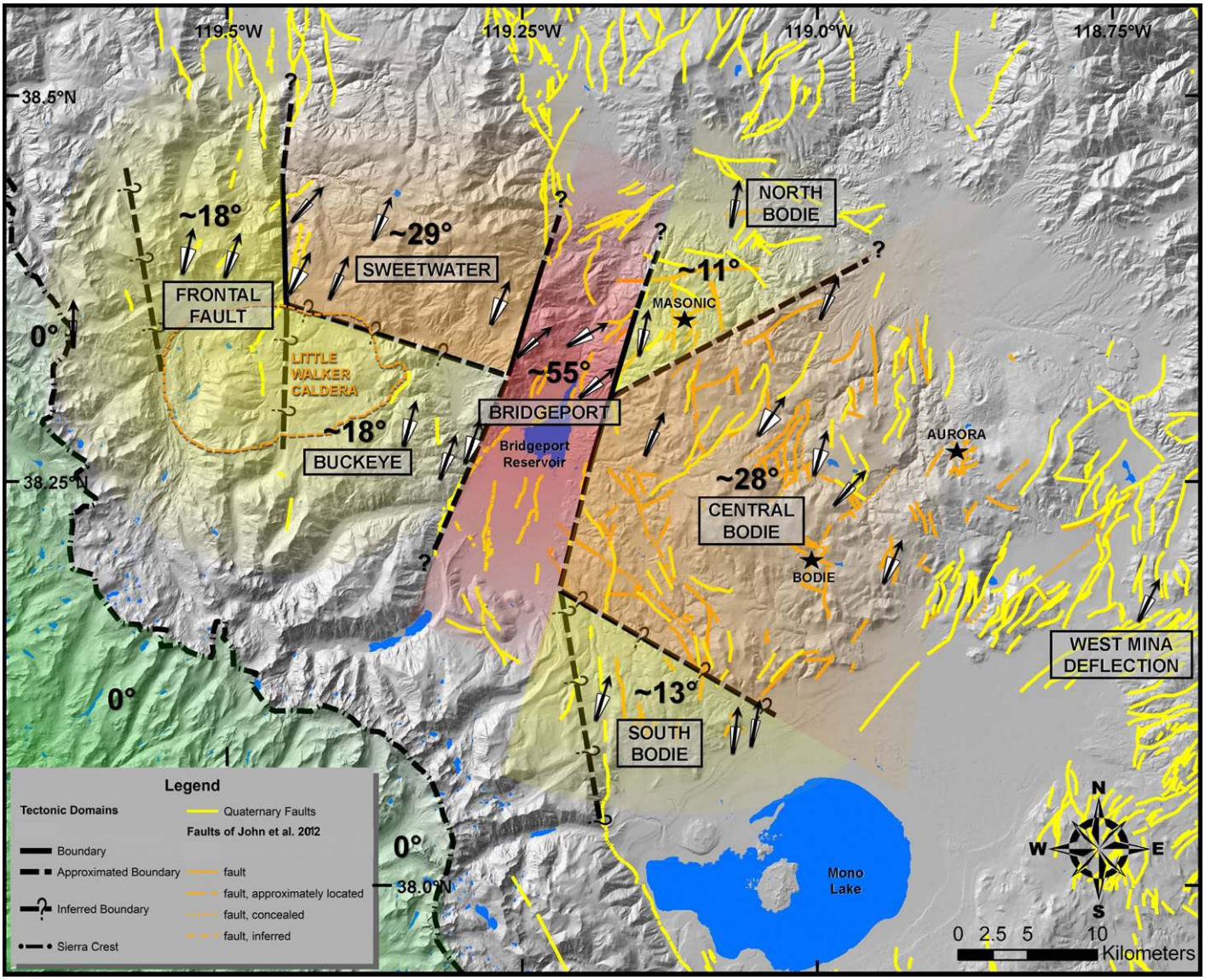


**Figure 8. Homogenized rotational domains defined by this study; domain names are in boxes and mean vertical-axis rotation magnitudes are in bold numerals. Stars denote location of mineral veining and mining districts from John et al. (2012). Arrows represented in red in Figure 7 using the Upper member reference directions of King et al. (2007) are in black after recalculation using our corrected reference directions for these units.**

## DISCUSSION

Here we first group localities into domains of similar rotation magnitude, and describe the boundaries which separate some of these domains. We then discuss styles and rates of deformation in the study area, and provide an alternative interpretation of data used in a previous study to infer constant rates of vertical-axis rotation. This is followed by a discussion of inferred paleostress orientations and rotation-accommodating structures for the Sweetwater Mountains and Bodie Hills, and then we present a kinematic model that accounts for mean magnitudes of vertical-axis rotation, mapped and inferred structures, regional physiography, and changes in deformation styles over time.

### Rotational Domains

The vertical-axis rotations used in this study from our new and previous paleomagnetic analyses reveal multiple discrete domains within which blocks have rotated similar magnitudes (Fig. 8; Table 4). This model simplifies the heterogeneous rotations evident in this study for greater understanding and modeling of regional kinematics. Domains were defined by groups of localities that were spatially contiguous and showed similar rotation magnitudes, while taking into consideration local faults, depositional basins, and/or linear trends in physiography (Fig. 8). Distinctive tectonic or geomorphic features were not always present between rotational domains inferred in this study. In addition, changes in rotation magnitudes may be more gradational in nature across domain boundaries; for that reason, we used solid, dashed, and dash-queried lines to represent our relative level of uncertainty to domain boundary position and/or existence (Fig. 8).

TABLE 4. DOMAIN MEAN ROTATIONS

| Domain name | Sampled site identification | Unit | Rotation (°) | Mean rotation* (°) |
|---|---|---|---|---|
| Frontal Fault | GM | Tseb | 22.3 ± 6.2 | 18 |
| | LW92 | Tseb | 13.3 ± 7.9 | |
| Sweetwater | TFR | Tset | 44.7 ± 6.8 | 29 |
| | MFO | Tseu | 25.9 ± 13.9 | |
| | LW23 | Tseb | 26.9 ± 11.0 | |
| | LW96 | Tseu | 25.7 ± 12.5 | |
| | BC | Tset | 23.4 ± 6.2 | |
| Buckeye | PC | Tseb | 15.4 ± 4.7 | 18 |
| | BDC | Tset | 19.3 ± 8.6 | |
| | LW93 | Tseb | 19.8 ± 7.7 | |
| Bridgeport | BOC | Tset | 48.7 ± 6.1 | 55 |
| | EWE | Tset | 60.0 ± 10.8 | |
| | MMC | Tseu | 55.2 ± 12.4 | |
| North Bodie | CHE | Tset | 11.7 ± 7.9 | 11 |
| | RRC | Tset | 9.8 ± 5.8 | |
| Central Bodie | HM | Tset | 22.9 ± 8.7 | 28 |
| | RSP | Tset | 23.8 ± 6.3 | |
| | HWC | Tset | 34.6 ± 17.0 | |
| | PLY | Tseb | 16.3 ± 8.1 | |
| | ATC | Tset | 42.8 ± 6.0 | |
| | LW88 | Tset | 22.9 ± 10.7 | |
| South Bodie | 3V156 | Tseu | 20.4 ± 12.5 | 13 |
| | LW86 | Tset | 6.6 ± 8.8 | |
| | 3V138 | Tset | 10.7 ± 6.5 | |
| West Mina Deflection | 3V129 | Tset | 26.2 ± 7.9 | 26 |

*Note:* Same sample sites as in Figure 7 and Table 3. Unit labels: Tset—Tollhouse Flat Member of the Eureka Valley Tuff (EVT); Tseb—By-Day Member of EVT; Tseu—Upper member of EVT.

*Average of site rotation in each domain, approximate.

This led to the recognition of two principal rotational domains, each displaying a mean vertical-axis rotation of ~29° and ~28° clockwise for the Sweetwater and Central Bodie domains, respectively (Fig. 8; Table 4). Positioned between these two principal domains was the Bridgeport domain, with a mean magnitude of ~55° clockwise rotation (Fig. 8; Table 4). This north-northeast–oriented corridor of large rotations included the wedge-shaped Bridgeport basin (Fig. 8). Several additional domains and their respective boundaries were inferred adjacent to the Sweetwater and Central Bodie domains based on lower mean magnitudes of ~11°–18° clockwise rotation (Fig. 8; Table 4). Details of these domains and their respective boundaries are addressed systematically in the following, from west to east across the study region (Fig. 8).

Located immediately east of the Sierran crest and west of the Sweetwater Mountains is the Frontal Fault domain of ~18° clockwise rotation (Fig. 8; Table 4). The western boundary of this domain is inferred to be within the series of Sierra frontal system normal faults (e.g., Chango Lake fault; Busby et al., 2008, 2013b). The eastern boundary of the Frontal Fault domain is defined by the north-south–oriented Sonora Junction fault and the linear drainage of the West Walker River (Busby et al., 2008; Fig. 8). Compared to the approximated or inferred boundaries of other adjacent domains discussed herein, this eastern boundary is very well constrained by sampling proximity, mapped faults, and local physiography. The Sweetwater domain displays ~29° of clockwise rotation and abuts the Frontal Fault domain along the West Walker River (Fig. 8). The northeast-striking eastern boundary of the Sweetwater domain is best constrained along the linear drainage separating the Murphy Flat overlook and Boone Canyon sample localities (Figs. 7 and 8). This domain boundary is inferred to extend to the southwest along segments of the Robinson Creek fault (Fig. 2) and the northwest edge of the southern Bridgeport Valley (i.e., Bridgeport domain; Fig. 8). The southern end of this boundary also constrains the eastern edge of the Buckeye domain, which was based on three similarly clockwise-rotated sample localities situated directly west of Bridgeport Reservoir (Fig. 8). The Buckeye domain is located directly south of the Sweetwater domain, and is named for Buckeye Creek which flows into the southwest corner of Bridgeport Valley. The boundary between the main Sweetwater and the Buckeye domain is inferred along an approximately east-west–oriented linear valley, exploited by highway engineers for U.S. 395 (Figs. 3 and 8). The close proximity of sample sites in the Buckeye domain, their overlapping rotational errors, and the difference with rotation magnitudes of Sweetwater domain sites demonstrates that Buckeye sites are distinct from the Sweetwater domain. However, the distinction between the Buckeye and Frontal Fault domains is speculative; these were separated simply due to the lack of data within the Little Walker caldera. Future work may show them to be a single domain. As noted, the measured vertical-axis rotations for the Frontal Fault, Sweetwater, and Buckeye domains are of particular significance as these regions were previously considered to be unrotated since Eureka Valley Tuff emplacement (King et al., 2007; Rood et al., 2011).

The Bridgeport Valley is a distinctive physiographic and tectonic boundary between the Bodie and Sweetwater domains (Fig. 8). We include it in the Bridgeport domain, a region of higher rotation magnitude compared to adjacent domains. The valley forms a triangular extensional basin that has been infilled by Quaternary and older glacial, fluvial, and lacustrine sediments (Fig. 8). The largest vertical-axis rotations measured in this study were located north of the Bridgeport Reservoir (~50°–60°; Table 4), where the East Walker River exits the valley at its narrowest extent (Fig. 8). With relatively few constraints, we place the boundary between the Bridgeport domain and adjacent North, Central, and South Bodie domains (Fig. 8) along the edge of Bridgeport Valley.

Localities from the Central Bodie domain yield a mean magnitude of ~28° clockwise rotation (Fig. 8; Table 4). North and south of the Central Bodie domain are regions that apparently underwent little post–Late Miocene rotation (North Bodie and South Bodie domains, respectively; Fig. 8; Table 4). Rotation data provide little constraint on the position of the boundary between the North Bodie and Central Bodie domains, due to the large gap in the distribution of sample localities. Nonetheless, this boundary is considered to be fairly well defined based on a change in mapped Quaternary fault orientations. Faults to the northwest of the North Bodie–Central Bodie domain boundary are predominantly oriented northwest-southeast, whereas fault orientations to the south (in the Central Bodie domain) are northeast-southwest and maintain this general orientation (i.e., structural grain) southeast into the West Mina Deflection domain (Fig. 8). The southern edge of the Central Bodie domain is poorly constrained due to a large gap in the southwestern Bodie Hills sample localities and insufficient

physiographic or geologic evidence to indicate a possible structural boundary (Fig. 8). Sampling at the Murphy Spring locality was intended to better constrain the location of this boundary, but the site tilt-corrected mean remanence direction was considered to be unreliable based on restored inclination (see Results discussion; MSP, Fig. 7). Without additional data it is not possible to distinguish whether the transition between South and Central Bodie domains is a distinct boundary or a gradational zone (Fig. 8). Future paleomagnetic sampling within the study region has the potential to improve constraints on rotational domains and the nature of the boundaries that define them. The southwestern boundary of the South Bodie domain is speculatively placed along the northern strand of the Mono Lake frontal fault, with no constraints on the rotation on the Sierra side of this boundary.

Given the 11°–55° of rotation in different domains of the region since Eureka Valley Tuff emplacement ca. 9.5 Ma, the time-averaged rotation in the study area is 1.2°–5.8° m.y.$^{-1}$, depending upon location. Because this result is based on paleomagnetic results from only one time horizon, geologic, geophysical, and geodetic data may assist in evaluating whether this rotation rate has been steady, accelerating, decelerating, or more complex.

## Deformation History of the West-Central Walker Lane

The Frontal Fault, Buckeye, and South Bodie domains display mean magnitudes of clockwise vertical-axis rotation on the order of ~13°–18°, and are between the Sierra Nevada microplate and two rotational domains, Sweetwater and Central Bodie, which display approximately double the magnitude of mean rotation (~28°–29° clockwise; Table 4; Fig. 8). This pattern of deformation may require a more complicated kinematic model than the well-defined, regional-scale, fault-bound block rotations involving Riedel shear proposed for other portions of the Walker Lane (e.g., Faulds et al., 2005; Wesnousky, 2005). The eastward-increasing rotations observed in the study region may best be explained by lithospheric-scale, heterogeneous, simple shear where brittle upper crust is a discretized version of ductile shearing at depth. Such a regional relationship would be analogous to the quasi-continuum model of Sonder et al. (1994), wherein magnitudes of rotation increase moving toward the center of the deforming region, in this case the Walker Lane. Those regions immediately adjacent to the Sierra Nevada that have undergone little to no vertical-axis rotation likely represent the edge of the deformed zone. This would place the underlying boundary of ductile shearing below the Sierra Nevada frontal fault system, and the westernmost low magnitudes of rotation, demarcating the Sierra Nevada microplate–Walker Lane boundary at this latitude (~38°N). It also suggests that progressive distribution of higher magnitudes of dextral shear is being accommodated to the east toward better defined, classic Walker Lane–style strike-slip fault systems.

Interpretation of present-day deformation in portions of the west-central Walker Lane varies among researchers. Rood et al. (2011) interpreted paleomagnetic data from the Bodie Hills to be consistent with constant rotation rates of 5° ± 2° m.y.$^{-1}$ since the Early-Middle Miocene (discussed in the following). However, geodetic studies and resultant models have calculated present-day vertical-axis rotation rates of ~1° m.y.$^{-1}$ or less (e.g., McCaffrey, 2002; Hammond et al., 2011; W. Hammond, 2013, written commun.). Similarly, seismogenic strain has been interpreted to indicate pure (within error) crustal thinning in the vicinity of Bridgeport Valley, inconsistent with significant present-day rotation (Unruh et al., 2003). The present-day, seemingly pure crustal thinning of Unruh et al. (2003) is not kinematically conducive to large (e.g., 5° m.y.$^{-1}$) ongoing rotation in the study area. In addition, studies of major Quaternary faults support predominantly dip-slip motions within the west-central Walker Lane (e.g., Clark et al., 1984; Hayes, 1985). The lack of documented currently active and prominent strike-slip faults in the west-central Walker Lane may require a vertical-axis rotational history different from other regions in the Walker Lane (e.g., active left-lateral faulting of the Mina deflection; Fig. 2). None of the forgoing constraints is permissive of accelerating rotation since the Miocene, so we consider two possibilities: (1) the constant 5° ± 2° rates of vertical-axis rotation since the Early-Middle Miocene proposed by Rood et al. (2011) and the likely unrecognized oblique components of strike-slip motion occurring on normal faults and/or unrecognized strike-slip faults that could permit such rotation; or (2) an older period of higher rates of vertical-axis rotation that was followed by a change in deformation associated with now dormant strike-slip faults and/or previous strike-slip fault systems currently undergoing predominantly normal dip-slip motion.

We offer an alternative interpretation of data from Rood et al. (2011) that call into question the constant-rotation-rate model. Andesite lavas and breccias of the Clearwater Creek sites that Rood et al. (2011) considered to be 12–20 m.y. old were actually dated as ca. 9.7 Ma and are similar in age to the Eureka Valley Tuff (John et al., 2012; D.A. John, 2012, written commun.). This would prevent constraint of rotation rates beyond the Late Miocene and instead argue for large spatial variations in the Rood et al. (2011) results, consistent with our results (e.g., 74° ± 8° in Clearwater Creek area on 9.7 Ma rocks and 42° ± 11° on 9.4–9.5 Ma Eureka Valley Tuff elsewhere in Bodie Hills). More important, we question the statistical significance of clockwise rotation of the Pliocene Beauty Peak basalt sites (Rood et al., 2011). Sampled sites from each of their three locations may represent some duplication of individual lava flows or multiple flows emplaced in a relatively short time (i.e., several centuries). This view is supported by the tightly grouped site directions and overlapping 95% confidence ellipses at each location; i.e., mean directions for Rood et al. (2011) sites BP1 and BP2 are statistically indistinguishable from one another, as are BP3 and BP4, and BP5–BP7. This alternatively could represent three different short-lived eruptions that each produced multiple cooling units, but only three independent readings of geomagnetic secular variation. The use of individual site directions (n = 7) by Rood et al. (2011), compared to a mean direction of sites (n = 3) herein, at each location creates an artificial increase in the n-value for virtual geomagnetic pole (VGP) dispersion calculations used to determine adequate sampling of this secular variation. In addition, the use of individual site directions (n = 7) resulted in heavier weighting of some repeated directions, skewing the VGP mean in the clockwise direction in this circumstance. We recalculate grouped site mean directions for BP1 and BP2 as dec. = 178.3°, inc. = –57.0°, $\alpha_{95}$ = 14.4°, BP3 and BP4 as dec. = 0.9°, inc. = 56.0°, $\alpha_{95}$ = 5.8°, and BP5–BP7 as dec. = 26.1°, inc. = 57.8°, $\alpha_{95}$ = 5.4°. Our recalculations of Rood et al. (2011) Beauty Peak Basalt site grouped by location (n = 3) are dec. = 8.2°, inc. = 57.5°, $\alpha_{95}$ = 12.7° with VGP of lat = 83.5°, long = 329.4°, $\alpha_{95}$ = 18.6°. This produces a lower than expected dispersion (S = 12.1), compared to the expected dispersion of the geomagnetic field (e.g., S = 16; Merrill and McElhinny, 1983; McElhinny and McFadden, 1997), implying inadequate sampling of secular variation for these published Beauty Peak data. In addition, the mean VGP determined herein (n = 3) is statistically indistinguishable from the North America Miocene reference pole of Hagstrum et al. (1987) used by Rood et al. (2011). We infer this result to represent no statistically significant vertical-axis rotation of the Beauty Peak basalt at these locations since the Pliocene. Thus, closer scrutiny of the Rood et al. (2011) data does not support constant vertical-axis rotation of Bodie Hills since the Early Miocene, while still potentially being within their model error, which accommodates a "change of

the rotation rate by a factor of two" since the Pliocene (p. 15). The lack of statistically significant rotation in Pliocene volcanics supports a hypothesis of present-day low or no rotation and better fits geodetically determined present-day rotation rates (~1 m.y.$^{-1}$). Therefore, older and higher rates of rotational deformation are necessary to accommodate the magnitudes of vertical-axis rotation measured in the study area.

John et al. (2012) inferred changes in Miocene regional principal stresses at three different times from mineralized veins and faulting at three mining districts within the Bodie Hills (Fig. 8). Ages of strain indicators for the Masonic, Aurora, and Bodie mining districts allowed examination of temporal variation of principal-stress axes in the Bodie Hills immediately before, during, and immediately after passage of the Mendocino Triple Junction (John et al., 2012; Fig. 9). Changes in regional stress due to migration of the Mendocino Triple Junction are plausible given that the southern edge of the subducting Gorda plate is inferred to have been at the latitude of the central Walker Lane ca. 10 Ma (~38°N; Atwater and Stock, 1998; Jones et al., 2004). Because regional vertical-axis rotations modify strain-indicator orientations, corrections are required for interpretation of Middle-Late Miocene principal stresses in the Bodie Hills. We restore the principal-stress directions inferred from strain indicators to an inferred paleo-orientation by applying a counterclockwise back rotation around a vertical axis to each mining district (John et al., 2012; Fig. 9). Because there were no sampled sites located immediately within the mining districts, the amount of applied back rotation was determined by the average rotation of the domain containing the mining district (see Fig. 8 for mining district locations). Because these back rotations are based on magnitudes measured from ca. 9.4 Ma members of the Eureka Valley Tuff, the resultant principal-stress directions may have been slightly underrotated or overrotated into their inferred paleo-orientations when considering the age of strain indicators. Any magnitude of underrotation or overrotation of these mining districts is considered negligible for purposes of this study.

Two differences of inferred principal-stress directions were evident upon restoration of strain indicators into paleo-orientations. First, between ca. 13 and 10.3 Ma there was a slight shift in direction of maximum extension from east-southeast–west-northwest to east-west. This difference in principal-stress direction could be attributed to spatial variations in the overall stress field between the North and Central Bodie domains, and/or errors within determined directions used for mining district counterclockwise back rotation. Second, while the direction of maximum extension ($\sigma_3$) for the Aurora district at 10.3 Ma maintains a subparallel orientation to maximum extension of the Bodie district at 8.4 Ma, there is a distinct exchange between intermediate ($\sigma_2$) and maximum ($\sigma_1$) principal-stresses (John et al., 2012; Fig. 9). This swapping of $\sigma_1$ and $\sigma_2$ is indicative of a change in the regional deformation from a regime of strike-slip to normal faulting. McIntyre (1990) and Surpless (2011) documented a period of dextral and oblique slip on the Cottonwood Springs and Penrod Canyon faults in the northern Wassuk Range that terminated ca. 7 Ma. This termination in strike-slip deformation is approximately synchronous with change in the regional stress field as inferred from the Aurora and Bodie mining districts. Unlike the northern Wassuk paleo–slip history, the Bodie Hills lack evidence of any potential rotation-accommodating structures, perhaps because they are obscured beneath latest Miocene and Pliocene volcanics. Despite the lack of surface evidence for such structures, John et al. (2012) noted, from magnetic and gravity anomalies, several northeast- and west-northwest–oriented crustal lineaments within the pre-Tertiary basement. These lineaments may represent potential structures capable of accommodating vertical-axis rotation, and are now obscured by younger volcanic deposits in the study area.

It is possible that mapped faults in the study region reflect both old, inactive structures as well as active ones that formed more recently in the current tectonic regime. Alternatively, recent faulting may have reactivated Late Miocene structures responsible for the large measured rotations reported here. In this case, these structures, having previously rotated into their current positions, are presumably now oriented in directions favorable to accommodating present-day normal faulting. Nur et al. (1986, Fig. 4 therein) proposed, based on a transpressional model, that the propagation of new fault segments occurs when rotations reach a magnitude of ~45°. Our study modified this transpressional model by applying a transtensional stress to rotate blocks following a bookshelf and/or pinned-block model (e.g., McKenzie and Jackson, 1983; Nur et al., 1988; Luyendyk, 1991). Structures originally striking in a more northern orientation, similar in orientation to present-day Walker Lane dextral faulting and/or frontal faults (see Fig. 2), would have rotated into a more northeastern orientation perpendicular to present-day maximum extension (Fig. 10). In the pinned-block model the spaces that open between fault-bound blocks represent footwall exhumation on oblique-normal faults (Fig. 10). The Robinson Creek fault, which forms the northwest boundary of the Bridgeport Valley, may represent one of these primary structures reoriented in this way (Figs. 2 and 8). Similar accommodating structures within the Sweetwater Mountains and Bodie Hills may now be obscured by younger lithologies and are no

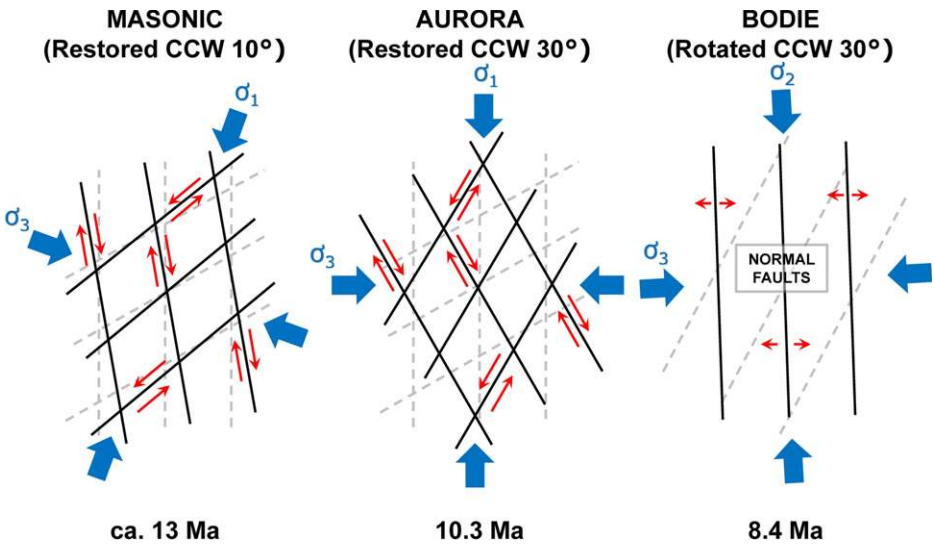


**Figure 9. Bodie Hills mining districts, associated mineralized structures, and inferred paleo-stress directions adapted from John et al. (2012). Mining district locations as in Figure 8. Counterclockwise (CCW) restored orientations are based on paleomagnetically determined magnitudes of clockwise vertical-axis rotations since ca. 9.4 Ma. Light gray dashed lines in background represent present-day in situ orientations. Red arrows depict relative motions for strike-slip faults, and undifferentiated extensional motion for normal faults.**

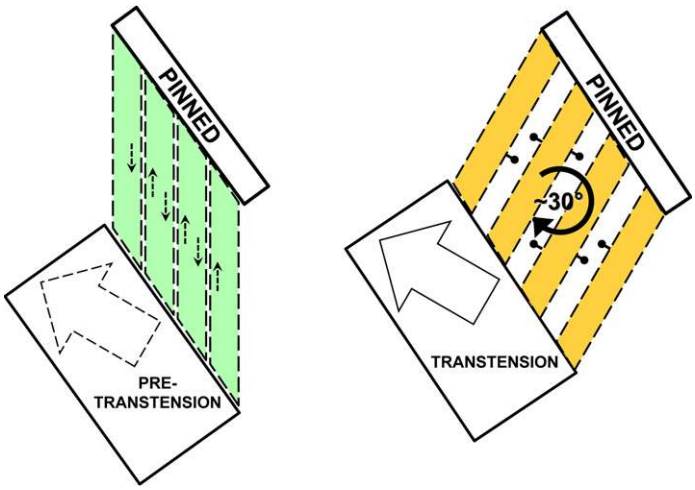


**Figure 10. Pinned-style block rotations in transtensional setting. Dashed arrows depict incipient motions (left side). Note the orientation of structures rotated (30°) perpendicular to direction of maximum extension (block arrow on transtension block; right side), and modification to predominantly dip-slip motions (ball and bar). Note that the rotating block ends are represented to have internally deformed, rather than rigidly forming small wedge-shaped basins at block ends. See text for further discussion.**

longer clearly evident beyond geophysical data (e.g., John et al., 2012). We consider, and present here, an evolution from strike-slip to normal motions of regional faulting as the favorable method of accomplishing vertical-axis rotations prior to the present-day normal fault motions and crustal thinning that are geologically constrained in the region (e.g., Brem, 1984; Clark et al., 1984; Hayes, 1985; Unruh et al., 2003; John et al., 2012).

## Kinematic Model

The kinematic model presented here addresses basic geologic, paleomagnetic, and regional physiographic constraints, while simplifying very complex deformation in the west-central Walker Lane. In accounting for these constraints, we intend to capture the fundamentals of crustal deformation not only in this study region, but similar transtensional regions in the world.

Considerations for our kinematic model are not limited solely to rotational domains, but also consider edge effects of rotating domains. Similar to tectonically controlled wedge-shaped basins noted in portions of the northern and central Walker Lane and Mina deflection (e.g., Wesnousky, 2005; Jayko and Bursik, 2012; Wesnousky et al., 2012), the wedge-shaped basins within the west-central Walker Lane appear to mimic the magnitudes of vertical-axis rotation determined for the Sweetwater and Bodie domains. The basins of Antelope and Bridgeport Valley are of similar size and shape and consistent with expected edge effects formed by rotational opening in response to the clockwise rotation of the Sweetwater domain occurring under regional transtension (Figs. 2 and 11). We hypothesize that the wedge shapes of these asymmetrical depositional basins have been controlled by differential slip along basin-bounding faults. In addition, asymmetric basin formation may accommodate more transtensional deformation compared to their rotating block counterparts. This variability in strain partitioning of transtension is evident where the ~30° southwest-facing angular opening of the Bridgeport basin and the highest magnitude rotations measured in the study area (~50°–60°) are in the same domain (i.e., Bridgeport domain; Fig. 8). Therefore, asymmetric basins may play a significant role in the accommodation of dextral shear in this and other parts of the Walker Lane (Wesnousky, 2005; Jayko and Bursik, 2012; Wesnousky et al., 2012).

Whereas post–Stanislaus Group vertical-axis rotation magnitudes vary across the study region, the majority of the study region is rotated ~30° clockwise; this value is adopted here to develop our simplified kinematic model. The Sweetwater Mountains and Bodie Hills represent the two major tectonic domains that kinematically accommodated ~30° of vertical-axis rotation by similar rotation of multiple blocks in each region. Adjacent to these domains are several significant depositional basins (e.g., Antelope Valley, Bridgeport Valley, and Mono Lake; Figs. 2 and 7) that represent zones of higher deformation between quasi-coherent rotational domains and adjacent low- or no-rotation domains. Thus, block rotation and basin opening have acted in concert to accommodate regional deformation since the Late Miocene. In our model, the Sierra Nevada microplate is defined as a fixed (i.e., pinned) region used to infer kinematic block motions within the west-central Walker Lane (Figs. 11A, 11B). Although vertical-axis rotations were measured in the Anchorite Hills and Excelsior Mountains (i.e., Mina deflection) to the east-southeast of the study area (King et al., 2007; Ferranti et al., 2009; Petronis et al., 2009), these rotations are not kinematically addressed in our simplified block model, because they are separated from the study region by the Mono Lake depositional basin and southern end of the Wassuk Range (Fig. 11). Similar to the Anchorite Hills–Excelsior Mountains, the Wassuk Range and Pine Grove Hills to the east and north of the study area, respectively, are included solely as translating blocks in our kinematic model, due to a lack of vertical-axis rotation data for those regions (Fig. 11B). Beyond the potential impingement with the southern tip of the Pine Grove Hills block along the northern Bodie Hills, the translation of nonrotating blocks (i.e., Pine Grove Hills, Wassuk Range, and Anchorite–Excelsior Mountains) has no kinematic effects on the model, and are mainly included to aid in visualization of predeformation and postdeformation geography (Figs. 11A, 11B).

The kinematic block model presented here restores the present-day block geometry and physiography to an inferred pre–Late Miocene configuration with only minor block length modification to the long axis of the rotating blocks (Fig. 11). Applying the inferred maximum principal stresses of John et al. (2012) oriented approximately north-northeast–south-southwest for the Bodie Hills (ca. 13–10.8 Ma), an initial configuration of parallel incipient structures was positioned in an approximately conjugate orientation for the Sweetwater and Bodie Hills (Fig. 11A). For the Sweetwater Mountains, we have chosen the conjugate set of incipient structures based on ~30° counterclockwise back rotation of present-day mapped faults (Brem, 1984). This incipient orientation is subparallel to present-day faults of the Sierra Nevada frontal fault system (e.g., Busby et al., 2013b; Fig. 11C). Similarly incipient structures in the Bodie Hills (Fig. 11A) are based on ~30° counterclockwise back rotation of present-day and geophysically inferred structures (John et al., 2012). These prerotational faults and principal-stress axis

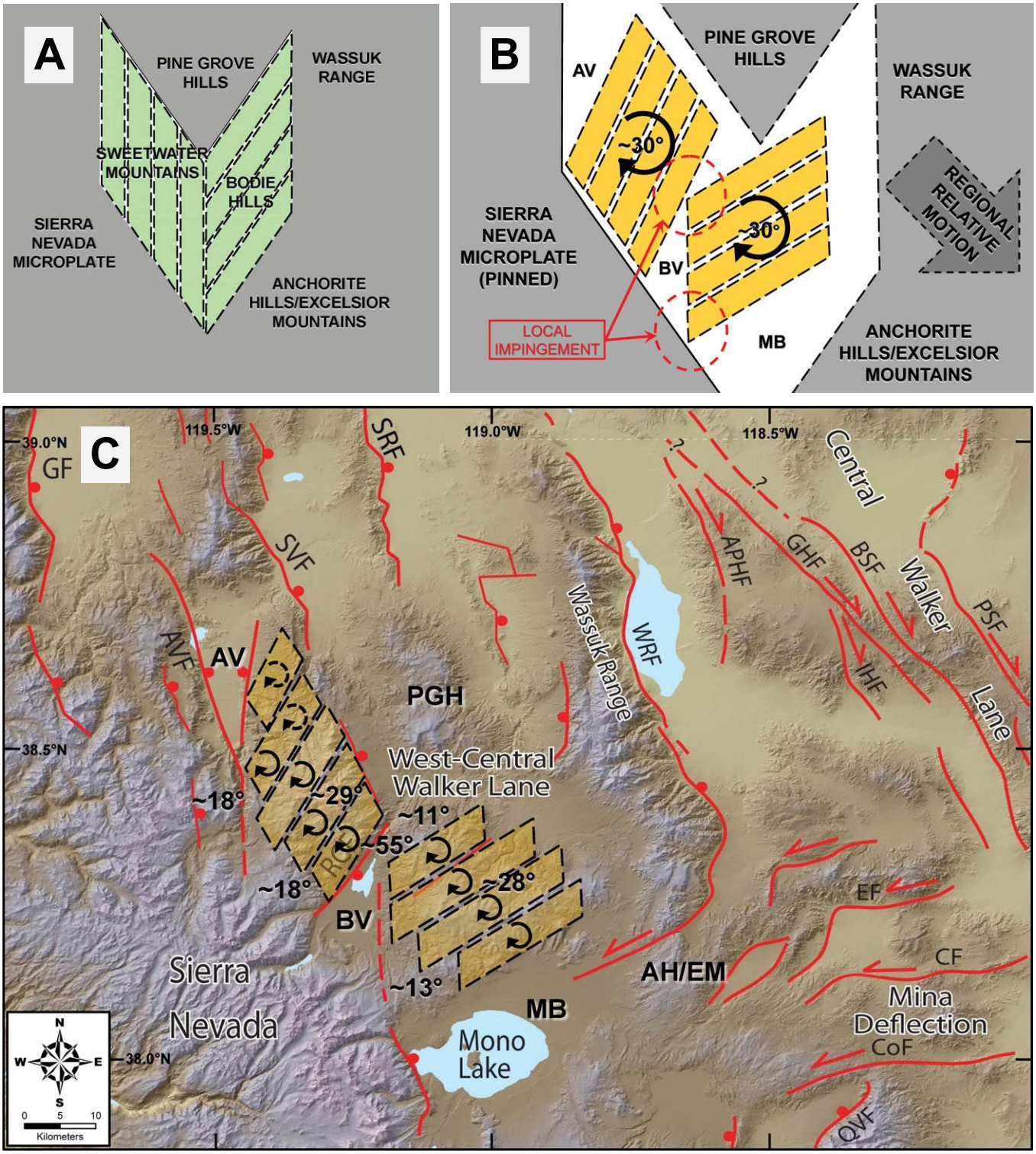


**Figure 11. The simplified kinematic block model presented permits the formation of asymmetric valleys and regional physiography associated with vertical-axis rotation of structures in the Sweetwater Mountains and Bodie Hills. (A) Pretranstension model depicting present-day physiographic regions and incipient dextral shear–accommodating structures discussed in text. (B) Post-transtension and/or present-day model depicting rotation accommodation with Sierra Nevada microplate fixed (pinned) and nonrotating physiographic block translation to the southeast (large dashed arrow). AV—Antelope Valley; BV—Bridgeport Valley; MB—Mono Basin. (C) Regional figure of central Walker Lane with overlain study mean rotations (see Table 4), and tectonic block modified from Figure 11B. Clockwise rotation indicator within blocks dashed where inferred. Additional regional depositional basins and physiography: Anchorite Hills–Excelsior Mountains—AH/EM; PGH—Pine Grove Hills. Regional fault labels are as in Figure 2.**

configurations are also the same as noted previously in the text and visually conveyed in the mining district back rotations of Figure 8. The ~30° of clockwise rotation of structures within and bounding the Sweetwater and Bodie Hills would lead to northeast- and east-northeast–oriented structures that are characterized by the present-day structural grain in some parts of these domains as well as the opening of the triangular Antelope Valley, Bridgeport Valley, and Mono depositional basins (Fig. 11B). Present-day model fault block orientations are guided by existing mapped faults and geophysical lineaments. For example, the southeastern portion of the Sweetwater Mountains contains the Robison Creek fault and parallel faults mapped by Brem (1984) that set the ending orientation of the kinematic model in this region. Similarly, in the Bodie Hills, modeled fault structures parallel the geophysical lineaments inferred by John et al. (2012) and approximately east-northeast–west-southwest–oriented faults that appear to be parallel to and step southeast toward structures at the western edge of the Mina deflection (Fig. 11C). Two regions of impingement between domains are noted in the simplified block model (Fig. 11B). The first is between the Sweetwater and Bodie rotating blocks at the northern end of Bridgeport Valley. This is where the largest vertical-axis rotations were measured (~50°–60°). We suspect that these larger rotations occurred as the Bodie Hills moved southwestward along the southeast boundary of the Sweetwater Mountains (Fig. 11). The second impingement, at the southwest tip of the Bodie Hills domain, reflects a slight component of transpression inferred for the northern Mono Basin by Unruh et al. (2003).

## CONCLUSIONS

Mean paleomagnetic remanence directions from outcrops of the Stanislaus Group constrain the magnitudes of vertical-axis block rotations spanning the west-central Walker Lane. Several localities, each containing multiple Eureka Valley Tuff members, display rotational differences as high as ~30° between different Eureka Valley Tuff units of similar age when compared to previously published Eureka Valley Tuff reference directions. Rapid syndepositional rotation rates (>35° m.y.$^{-1}$) are unreasonable as the sole explanation for rotational differences between units at these sites, suggesting that existing paleomagnetic reference direction sites for the Upper member and By-Day Member (King et al., 2007) have undergone rotation and cannot be used for reference. This interpretation was verified by independently assessing the rotation of localities containing the By-Day Member and Upper member and then back rotating to calculate a corrected reference direction (By-Day Member, dec. = 353.2°, inc. = 43.7°, $\alpha_{95}$ = 10.8°; tentatively, Upper member, dec. = 335.0°, inc. = 30.5°, $\alpha_{95}$ = 6.1°). Our By-Day Member reference is derived from the difference in mean locality remanence directions of Stanislaus Group lavas (Pluhar et al., 2009) between Sonora Peak (n = 23) on the stable Sierra Nevada and Grouse Meadow (n = 16), which contains the By-Day Member, but is within a tectonically active region. We further verified this result by comparing the time-averaged VGP for Grouse Meadow to the Miocene North American reference pole (Hagstrum et al., 1987). Our corrected reference direction for the By-Day Member is supported by work at the Stanislaus Group type section on the stable Sierra Nevada microplate (Farner et al., 2012). The recognition and rectification of problematic reference directions for the Stanislaus Group revealed vertical-axis rotations in portions of the study area previously believed to be unrotated (e.g., Frontal Fault, Buckeye, and Sweetwater rotational domains, Fig. 8) as well as a pattern of rotation characterized by distinct domains of different rotation magnitudes since Stanislaus Group emplacement. Seven domains are inferred from similar paleomagnetic determined rotation magnitudes and spatial continuity data, i.e., Frontal Fault (~18°), Buckeye (~18°), Sweetwater (~29°), Bridgeport (~55°), North Bodie (~11°), Central Bodie (~28°), and South Bodie (~13°). Boundaries for these domains were defined by regional faults, depositional basins, and/or linear trends in physiography.

Both the Bodie Hills and Sweetwater Mountains are bound by depositional basins where regional deformation is likely concentrated. Two of these depositional basins (e.g., Antelope and Bridgeport Valleys) are triangular and open to angles similar in magnitude (~30°) to the post–Stanislaus Group rotation magnitude of the adjacent domains. These basins probably play a significant role, along with block rotations, in accommodating regional dextral shear. Changes in the inferred paleostress orientations from John et al. (2012) support a Late Miocene transition and/or modification of deformation style in the region of the Bodie Hills. A simplified rotating model of discrete fault systems is presented here to account for block kinematics and the accommodation of deformation in the region. Application of determined regional rotations (~30° clockwise) to incipient deformation accommodating structures proposed in the kinematic model resulted in block orientations and edge responses consistent with present-day physiography and fault orientations in the region.

This work reveals that the west-central Walker Lane consists of a complex assemblage of interacting and evolving domains and structures. The geometry and rotational histories of these domains support a model of regional dextral shear accommodation demonstrating that the west-central Walker Lane should be included as an important part of the Walker Lane transtensional accommodation zone. The results presented here not only improve understanding of deformation in the Walker Lane, but illuminate the potentially significant contribution of crustal block vertical-axis rotations in other transtensional regions of the world.

### ACKNOWLEDGMENTS

This study was partially supported through scholarships and grants from the Fresno Gem and Mineral Society, the Educational Employees Credit Union, and the College of Science and Mathematics, California State University, Fresno. We thank the Geophysical Unit Menlo Park (GUMP) of the U.S. Geological Survey (Menlo Park, California) for use of the Rock- and Paleo-magnetics Laboratory, and D. John, E. du Bray, R. Blakely, and S. Box for helpful discussions and reviews of data. The paper was significantly improved by the careful and detailed comments of reviewers P. Cashman and W. Hammond. We also acknowledge C. Busby, who as guest editor provided both opportunity and guidance in our contribution to this themed issue of *Geosphere*.

### REFERENCES CITED

Allmendinger, R.W., 2007, Strain and rotation rates from GPS; pitfalls and possibilities in the search for a permanent deformation signal: Geological Society of America Abstracts with Programs, v. 39, no. 6, p. 47.

Al Rawi, Y.T., 1969, Cenozoic history of the northern part of Mono Basin (Mono county): CA, NV [Ph.D. thesis]: Berkeley, University of California at Berkeley, 188 p.

Argus, D.F., and Gordon, R.G., 2001, Present tectonic motion across the Coast Ranges and San Andreas fault system in central California: Geological Society of America Bulletin, v. 113, p. 1580–1592, doi:10.1130/0016-7606(2001)113<1580:PTMATC>2.0.CO;2.

Atwater, T., and Stock, J., 1998, Pacific–North America plate tectonics of the Neogene southwestern United States—An update: International Geology Review, v. 40, p. 375–402, doi:10.1080/00206819809465216.

Bennett, R.A., Wernicke, B.P., Niemi, N.A., Friedrich, A.M., and Davis, J.L., 2003, Contemporary strain rates in the northern Basin and Range province from GPS data: Tectonics, v. 22, doi:10.1029/2001TC001355.

Brem, G.F., 1984, Geologic map of the Sweetwater Roadless Area, Mono County, California, and Lyon and Douglas Counties, Nevada: U.S. Geological Survey Miscellaneous Field Studies Map MF-1535-B, scale 1:62,500.

Busby, C.J., 2013, Birth of a plate boundary at ca. 12 Ma in the Ancestral Cascades arc, and implications for transtensional rift propagation, Walker Lane belt: Geosphere, v. 9, doi:10.1130/GES00928.1.

Busby, C.J., Hagan, J.C., Putirka, K., Pluhar, C.J., Gans, P.B., Wagner, D.L., Rood, D., DeOreo, S.B., and Skilling, I., 2008, The ancestral Cascades Arc; Cenozoic evolution of the central Sierra Nevada (California) and the birth of the new plate boundary, *in* Wright, J.E., and Shervais, J.W., eds., Ophiolites, arcs, and batholiths: A tribute to Cliff Hopson: Geological Society of America Special Paper 438, p. 331–378, doi:10.1130/2008.2438(12).

Busby, C.J., Koerner, A.K., Melosh, B.L., Hagan, J.C., and Andrews, G.D.M., 2013a, Sierra Crest graben-vent system: A Walker Lane pull apart within the ances-

tral Cascades arc: Geosphere, v. 9, p. 736–780, doi: 10.1130/GES00670.1.

Busby, C.J., Hagan, J.C., and Renne, P., 2013b, Initiation of Sierra Nevada range front–Walker Lane faulting ca. 12 Ma in the Ancestral Cascades arc: Geosphere, v. 9, doi: 10.1130/GES00927.1.

Cashman, P.H., and Fontaine, S.A., 2000, Strain partitioning in the northern Walker Lane, western Nevada and northeastern California: Tectonophysics, v. 326, p. 111–130, doi:10.1016/S0040-1951(00)00149-9.

Chapin, C.E., and Lowell, G.R., 1979, Primary and secondary flow structures in ash-flow tuffs of the Gribbles Run paleovalley, central Colorado, *in* Chapin, C.E., and Elston, W.E., eds., Ash-flow tuffs: Geological Society of America Special Paper 180, p. 137–154, doi: 10.1130/SPE180-p137.

Clark, M.M., and 12 others, 1984, Preliminary slip-rate table for late Quaternary faults of California: U.S. Geological Survey Open-File Report 84–106, 12 p.

Cogne, J.P., 2003, PaleoMac: A Macintosh (super TM) application for treating paleomagnetic data and making plate reconstructions: Geochemistry, Geophysics, Geosystems, v. 4, no. 1, 23 p.

DeCelles, P.G., 2004, Late Jurassic to Eocene evolution of the Cordilleran thrust belt and foreland basin system, western USA: American Journal of Science, v. 304, p. 105–168, doi:10.2475/ajs.304.2.105.

Demarest, H.H., 1983, Error analysis of the determination of tectonic rotation from paleomagnetic data: Journal of Geophysical Research, v. 88, p. 4321–4328, doi: 10.1029/JB088iB05p04321.

Dickinson, W.R., 2006, Geotectonic evolution of the Great Basin: Geosphere, v. 2, p. 353–368, doi: 10.1130/GES00054.1.

Dixon, T.H., Robaudo, S., Lee, J., and Reheis, M.C., 1995, Constraints on present-day Basin and Range deformation from space geodesy: Tectonics, v. 14, p. 755–772, doi:10.1029/95TC00931.

Dixon, T.H., Miller, M., Farina, F., Wang, H., and Johnson, D., 2000, Present-day motion of the Sierra Nevada block and some tectonic implications for the Basin and Range province, North American Cordillera: Tectonics, v. 19, p. 1–24, doi:10.1029/1998TC001088.

Dixon, T.H., Norabuena, E., and Hotaling, L., 2003, Paleoseismology and global positioning system: Earthquake-cycle effects and geodetic versus geologic fault slip rates in the eastern California shear zone: Geology, v. 31, p. 55–58, doi:10.1130/0091-7613(2003)031<0055:PAGPSE>2.0.CO;2.

England, P.C., and Wells, R.E., 1991, Neogene rotations and quasi-continuous deformation of the Pacific Northwest continental margin: Geology, v. 19, p. 978–981, doi: 10.1130/0091-7613(1991)019<0978:NRAQDO>2.3.CO;2.

Farner, M.J., Pluhar, C.J., Asami, R.T., Putirka, K.D., Busby, C.J., and Renne, P.R., 2012, Paleomagnetism, geochronology, and geochemistry of the type section of the Stanislaus Group: Reference parameters from the stable Sierra Nevada microplate, CA: American Geophysical Union proceedings, fall meeting, abs. GP21A–1141.

Faulds, J.E., and Henry, C.D., 2008, Tectonic influences on the spatial and temporal evolution of the Walker Lane: An incipient transform fault along the evolving Pacific–North American plate boundary, *in* Spencer, J.E., and Titley, S.R., eds., Ores and orogenesis: Circum-Pacific tectonics, geologic evolution, and ore deposits: Arizona Geological Society Digest 22, p. 437–470.

Faulds, J.E., and Perkins, M.E., 2007, Evidence for dextral shear along the western margin of the Carson Sink: The missing link between the central and northern Walker Lane, western Nevada: Geological Society of America Abstracts with Programs, v. 39, no. 4, p. 15.

Faulds, J.E., Henry, C.D., and Hinz, N.H., 2005, Kinematics of the northern Walker Lane: An incipient transform fault along the Pacific–North American plate boundary: Geology, v. 33, p. 505–508, doi:10.1130/G21274.1.

Ferranti, L., Oldow, J.S., Geissman, J.W., and Neil, M.M., 2009, Flattening strain during coordinated slip on a curved fault array, Rhodes Salt Marsh extensional basin, central Walker Lane, west-central Nevada, *in* Oldow, J.S., and Cashman, P.H., eds., Late Cenozoic structural and evolution of the Great Basin–Sierra Nevada transition: Geological Society of America Special Paper 447, p. 189–214, doi:10.1130/2009.2447(11).

Fisher, R.A., 1953, Dispersion on a sphere: Royal Society of London Proceedings, ser. A, v. 217, p. 295–305, doi: 10.1098/rspa.1953.0064.

Fredrickson, S.M., Lindeman, J.R., Pluhar, C.J., and Carlson, C.W., 2013, Kinematics of deformation in west-central Walker Lane; Paleomagnetic testing of fault-block rotation and doming models, eastern California and western Nevada: Geological Society of America Abstracts with Programs, v. 45, no. 6, p. 18.

Gordon, R.G., 1995, Plate motions, crustal and lithospheric mobility, and paleomagnetism; Prospective viewpoint: Journal of Geophysical Research, v. 100, no. B12, p. 24367–24392, doi:10.1029/95JB01912.

Gorny, C., Busby, C., Pluhar, C.J., Hagan, J., and Putirka, K., 2009, An in-depth look at distal Sierra Nevada palaeochannel fill: Drill cores through the Table Mountain Latite near Knights Ferry: International Geology Review, v. 51, p. 824–842, doi: 10.1080/00206810902944960.

Hagstrum, J.T., and Gans, P.B., 1989, Paleomagnetism of the Oligocene Kalamazoo Tuff; Implications for middle Tertiary extension in east central Nevada: Journal of Geophysical Research, v. 94, no. B2, p. 1827–1842, doi:10.1029/JB094iB02p01827.

Hagstrum, J.T., Sawlan, M.G., Hausback, B.P., Smith, J.G., and Grommé, C.S., 1987, Miocene paleomagnetism and tectonic setting of the Baja California Peninsula, Mexico: Journal of Geophysical Research, v. 92, no. B3, p. 2627–2639, doi:10.1029/JB092iB03p02627.

Hammond, W.C., Blewitt, G., and Kreemer, C., 2011, Block modeling of crustal deformation of the northern Walker Lane and Basin and Range from GPS velocities: Journal of Geophysical Research, v. 116, B04402, doi: 10.1029/2010JB007817.

Hardyman, R.F., 1984, Strike-slip, normal, and detachment faults in the northern Gillis Range, Walker Lane of west central Nevada, *in* Lintz, J., Jr., ed., Western geologic excursions, Volume 4: Geological Society of America Annual Meeting Guidebook: Reno, Nevada, Mackay School of Mines, p. 184–203.

Hayes, G.F., 1985, Late Quaternary deformation and seismic risk in the southern Sierra Nevada Great Basin boundary zone near the Sweetwater Mountains, California and Nevada [M.S. thesis]: Reno, University of Nevada, 135 p.

Henry, C.D., Faulds, J.E., Garside, L.G., and Hinz, N.H., 2003, Tectonic implications of ash-flow tuffs in paleovalleys in the western US: Geological Society of America Abstracts with Programs, v. 35, no. 6, p. 346.

Henry, C.D., McIntosh, W.C., McDowell, F.W., Lipman, P.W., Chapin, C.E., and Richardson, M.T., 2010, Distribution, timing, and controls of the mid-Cenozoic ignimbrite flareup in western North America: Geological Society of America Abstracts with Programs, v. 42, no. 5, p. 144.

Hillhouse, J.W., and Grommé, S., 2011, Updated paleomagnetic pole from Cretaceous plutonic rocks of the Sierra Nevada, California: Tectonic displacement of the Sierra Nevada block: Lithosphere, v. 3, p. 275–288, doi:10.1130/L142.1.

Huber, N.K., 1990, The late Cenozoic evolution of the Tuolumne River, central Sierra Nevada, California: Geological Society of America Bulletin, v. 102, p. 102–115, doi:10.1130/0016-7606(1990)102<0102:TLCEOT>2.3.CO;2.

Jayko, A.S., and Bursik, M., 2012, Active transtensional intracontinental basins: Walker Lane belt in the western Great Basin, *in* Busby, C.J., and Azor, A., eds., Tectonics of sedimentary basins: Recent advances: Oxford, UK, Wiley-Blackwell, p. 226–248.

John, D.A., du Bray, E.A., Blakely, R.J., Fleck, R.J., Vikre, P.G., Box, S.E., and Moring, B.C., 2012, Miocene magmatism in the Bodie Hills volcanic field, California and Nevada: A long-lived eruptive center in the southern segment of the ancestral Cascades arc: Geosphere, v. 8, p. 44–97, doi:10.1130/GES00674.1.

Jones, C.H., Unruh, J., and Sonder, L.J., 1996, The role of gravitational potential energy in active deformation in the southwestern United States: Nature, v. 381, p. 37–41, doi:10.1038/381037a0.

Jones, C.H., Farmer, G.L., and Unruh, J., 2004, Tectonics of Pliocene removal of lithosphere of the Sierra Nevada, California: Geological Society of America Bulletin, v. 116, p. 1408–1422, doi:10.1130/B25397.1.

Jones, S.A., Pluhar, C.J., and Farner, M.J., 2013, Correlation and analysis of paleochannels in the Sierra Nevada, California, as displayed by the Stanislaus Group; Towards updating late Cenozoic uplift estimates: Geological Society of America Abstracts with Programs, v. 45, no. 6, p. 17.

King, N.M., Hillhouse, J.W., Grommé, S., Hausback, B.P., and Pluhar, C.J., 2007, Stratigraphy, paleomagnetism and anisotropy of magnetic susceptibility of the Miocene Stanislaus Group, central Sierra Nevada and Sweetwater Mountains, California and Nevada: Geosphere, v. 3, no. 6, p. 646–666, doi: 10.1130/GES00132.1.

Kirschvink, J.L., 1980, The least-squares line and plane and the analysis of palaeomagnetic data: Royal Astronomical Society Geophysical Journal, v. 62, p. 699–718, doi:10.1111/j.1365-246X.1980.tb02601.x.

Kirschvink, J.L., Kopp, R.E., Raub, T.D., Baumgartner, C.T., and Holt, J.W., 2008, Rapid, precise, and high-sensitivity acquisition of paleomagnetic and rock-magnetic data: Development of a low-noise automatic sample changing system for superconducting rock magnetometers: Geochemistry, Geophysics, Geosystems, v. 9, Q05Y01, doi:10.1029/2007GC001856.

Koerner, A., Busby, C., Putirka, K., and Pluhar, C.J., 2009, New evidence for alternating effusive and explosive eruptions from the type section of the Stanislaus Group in the 'Cataract' palaeocanyon, central Sierra Nevada: International Geology Review, v. 51, p. 962–985, doi: 10.1080/00206810903028185.

Kreemer, C., Blewitt, G., and Hammond, W.C., 2009, Geodetic constraints on contemporary deformation in the northern Walker Lane: 2. Velocity and strain rate tensor analysis, *in* Oldow, J.S., and Cashman, P.H., eds., Late Cenozoic structural and evolution of the Great Basin–Sierra Nevada Transition: Geological Society of America Special Paper 447, p. 17–31, doi:10.1130/2009.2447(02).

Lamb, S.H., 1994, Behavior of the brittle crust in wide plate boundary zones: Journal of Geophysical Research, v. 99, no. B3, p. 4457–4483, doi:10.1029/93JB02574.

Lewis, J.C., Twiss, R.J., Pluhar, C.J., and Monastero, F.C., 2007, Multiple constraints on divergent strike-slip deformation along the eastern margin of the Sierran microplate, SE California, *in* Till, A.B., et al., eds., Exhumation associated with continental strike-slip systems: Geological Society of America Special Paper 434, p. 107–128, doi:10.1130/2007.2434(06).

Locke, A., Billingsley, P.R., and Mayo, E.B., 1940, Sierra Nevada tectonic patterns: Geological Society of America Bulletin, v. 51, p. 513–540.

Lonsdale, P., 1991, Structural patterns of the Pacific floor offshore of Peninsular California, *in* Dauphin, J.P., and Simoneit, B.T., eds., Gulf and Peninsula Province of the Californias: American Association of Petroleum Geologists Memoir 47, p. 87–125.

Luyendyk, B.P., 1991, A model for Neogene crustal rotations, transtension, and transpression in southern California: Geological Society of America Bulletin, v. 103, p. 1528–1536, doi:10.1130/0016-7606(1991)103<1528:AMFNCR>2.3.CO;2.

McCaffrey, R., 2002, Crustal block rotations and plate coupling, *in* Stein, S.A., and Freymueller, J., eds., Plate boundary zones: American Geophysical Union Geodynamics Series 30, p. 101–122, doi: 10.1029/GD030p0101.

McElhinny, M.W., and McFadden, P.L., 1997, Palaeosecular variation over the past 5 Myr based on a new generalized database: Geophysical Journal International, v. 131, p. 240–252, doi:10.1111/j.1365-246X.1997.tb01219.x.

McFadden, P.L., and McElhinny, M.W., 1988, The combined analysis of remagnetization circles and direct observations in palaeomagnetism: Earth and Planetary Science Letters, v. 87, p. 161–172, doi:10.1016/0012-821X(88)90072-6.

McIntosh, W.C., 1991, Evaluation of paleomagnetism as a correlation criterion for Mogollon-Datil ignimbrites,

southwestern New Mexico: Journal of Geophysical Research, v. 96, no. B8, p. 13,459–13,483, doi: 10.1029/91JB00603.

McIntyre, J.L., 1990, Late Cenozoic structure of the Central Wassuk Range, Mineral County, Nevada [M.S. thesis]: Corvallis, Oregon State University, 107 p.

McKenzie, D.P., and Jackson, J.A., 1983, The relationship between strain rates, crustal thickening, paleomagnetism, finite strain and fault movements within a deforming zone: Earth and Planetary Science Letters, v. 65, p. 182–202, doi:10.1016/0012-821X(83)90198-X.

Merrill, R.T., and McElhinny, M.W., 1983, The Earth's magnetic field: Its history, origin and planetary perspective: San Diego, California, Academic Press, 401 p.

Miller, M.M., Johnson, D.J., and Dixon, T.H., 2001, Refined kinematics of the eastern California shear zone from GPS observations, 1993–1998: Journal of Geophysical Research, v. 106, p. 2245–2263, doi: 10.1029/2000JB900328.

Murphy, J.J., Watkinson, A.J., and Oldow, J.S., 2009, Graphical analysis of divergence between GPS velocity and strain trajectory within the Walker Lane, Nevada, *in* Oldow, J.S., and Cashman, P.H., eds., Late Cenozoic structure and evolution of the Great Basin–Sierra Nevada transition: Geological Society of America Special Paper 447, p. 55–70, doi:10.1130/2009.2447(04).

Nicholson, C., Sorlien, C.C., Atwater, T., Crowell, J.C., and Luyendyk, B.P., 1994, Microplate capture, rotation of the western Transverse Ranges, and initiation of the San Andreas transform as a low-angle fault system: Geology, v. 22, p. 491–495, doi:10.1130/0091-7613(1994)022<0491:MCROTW>2.3.CO;2.

Noble, D.C., Slemmons, D.B., Korringa, M.K., Dickinson, W.R., Al Rawi, Y., and McKee, E.H., 1974, Eureka Valley Tuff, east-central California and adjacent Nevada: Geology, v. 2, p. 139–142, doi:10.1130/0091-7613(1974)2<139:EVTECA>2.0.CO;2.

Nur, A., Ron, H., and Scotti, O., 1986, Fault mechanics and the kinematics of block rotation: Geology, v. 14, p. 746–749, doi:10.1130/0091-7613(1986)14<746:FMATKO>2.0.CO;2.

Nur, A., Ron, H., and Scotti, O., 1988, Mechanics of distributed fault and block rotation, *in* Kissel, C., and Laj, C., eds., Paleomagnetic rotations and continental deformation: Dordrecht, Kluwer Academic Publishers, Nato ASO series C, v. 254, p. 209–228.

Oldow, J.S., 2003, Active transtensional boundary zone between the western Great Basin and Sierra Nevada block, western U.S. Cordillera: Geology, v. 31, p. 1033–1036, doi:10.1130/G19838.1.

Oldow, J.S., Aiken, C.L.V., Hare, J.L., Ferguson, J.F., and Hardyman, R.F., 2001, Active displacement transfer and differential block motion within the central Walker Lane, western Great Basin: Geology, v. 29, p. 19–22, doi:10.1130/0091-7613(2001)029<0019:ADTADB>2.0.CO;2.

Oldow, J.S., Geissman, J.W., and Stockli, D.F., 2008, Evolution and strain reorganization within late Neogene structural stepovers linking the central Walker Lane and northern Eastern California Shear Zone, western Great Basin: International Geology Review, v. 50, p. 270–290, doi:10.2747/0020-6814.50.3.270.

Oskin, M., and Stock, J., 2003, Marine incursion synchronous with plate boundary localization in the Gulf of California: Geology, v. 31, p. 23–26, doi:10.1130/0091-7613(2003)031<0023:MISWPB>2.0.CO;2.

Petronis, M.S., Geissman, J.W., Oldow, J.S., and McIntosh, W.C., 2002, Paleomagnetic and $^{40}Ar/^{39}Ar$ geochronologic data bearing on the structural evolution of the Silver Peak extensional complex, west-central Nevada: Geological Society of America Bulletin, v. 114, p. 1108–1130, doi:10.1130/0016-7606(2002)114<1108:PAAAGD>2.0.CO;2.

Petronis, M.S., Geissman, J.W., Oldow, J.S., and McIntosh, W.C., 2007, Tectonic summary of the southwest Silver Peak Range, Central Walker Lane, NV: Paleomagnetic and geochronologic data, *in* Till, A., et al., eds., Exhumation associated with continental strike-slip fault systems: Geological Society of America Special Paper 434, p. 81–106, doi:10.1130/2007.2434(05).

Petronis, M.S., Geissman, J.W., Oldow, J.S., and McIntosh, W.C., 2009, Late Miocene to Pliocene vertical-axis rotation attending development of the Silver Peak–Line Mountain displacement transfer zone, west-central Nevada, *in* Oldow, J.S., and Cashman, P.H., eds., Late Cenozoic structure and evolution of the Great Basin–Sierra Nevada transition: Geological Society of America Special Paper 447, p. 215–254, doi:10.1130/2009.2447(12).

Pluhar, C.J., Coe, R.S., Lewis, J.C., Monastero, F.C., and Glen, J.M.G., 2006, Fault block kinematics at a releasing stepover of the Eastern California Shear Zone; partitioning of rotation style in and around the Coso geothermal area and nascent metamorphic core complex: Earth and Planetary Science Letters, v. 250, p. 134–163, doi:10.1016/j.epsl.2006.07.034.

Pluhar, C.J., Deino, A.L., King, N.M., Busby, C., Hausback, B.P., Wright, T., and Fisher, C., 2009, Lithostratigraphy, magnetostratigraphy, and radiometric dating of the Stanislaus Group, CA, and age of the Little Walker Caldera: International Geology Review, v. 51, p. 873–899, doi:10.1080/00206810902945017.

Priest, G.R., 1979, Geology and geochemistry of the Little Walker volcanic center, Mono County, California [Ph.D. thesis]: Corvallis, Oregon State University, 253 p.

Ransome, F.L., 1898, Some lava flows of the western slope of the Sierra Nevada, California: U.S. Geological Survey Bulletin 89, 74 p.

Rood, D.H., Burbank, D.W., Herman, S.W., and Bogue, S., 2011, Rates and timing of vertical-axis block rotations across the central Sierra Nevada–Walker Lane transition in the Bodie Hills, California/Nevada: Tectonics, v. 30, doi:10.1029/2010TC002754.

Slemmons, D.B., 1953, Geology of the Sonora Pass region [Ph.D. thesis]: Berkeley, University of California, 222 p.

Slemmons, D.B., 1966, Cenozoic volcanism of the central Sierra Nevada, California, *in* Bailey, E.H., ed., Geology of northern California: California Division of Mines and Geology Bulletin 190, p. 199–208.

Sonder, L.J., Jones, C.H., Salyards, S.L., and Murphy, K.M., 1994, Vertical axis rotations in the Las Vegas Valley shear zone, southern Nevada: Paleomagnetic constraints on kinematics and dynamics of block rotations: Tectonics, v. 13, p. 769–788, doi:10.1029/94TC00352.

Stewart, J.H., 1988, Tectonics of the Walker Lane belt, western Great Basin: Mesozoic and Cenozoic deformation in a zone of shear, *in* Ernst, W.G., ed., Metamorphism and crustal evolution of the western United States: Englewood Cliffs, New Jersey, Prentice Hall, p. 681–713.

Surpless, B.E., 2008, Modern strain localization in the central Walker Lane, western United States: Implications for the evolution of intraplate deformation in transtensional settings: Tectonophysics, v. 457, p. 239–253, doi:10.1016/j.tecto.2008.07.001.

Surpless, B.E., 2011, Cenozoic tectonic evolution of the central Wassuk Range, western Nevada, USA: International Geology Review, v. 54, p. 547–571, doi: 10.1080/00206814.2010.548117.

Thatcher, W., 1995, Microplate versus continuum descriptions of active tectonic deformation: Journal of Geophysical Research, v. 100, no. B3, p. 3885–3894, doi: 10.1029/94JB03064.

Unruh, J., Humphrey, J., and Barron, A., 2003, Transtensional model for the Sierra Nevada frontal fault system, eastern California: Geology, v. 31, p. 327–330, doi: 10.1130/0091-7613(2003)031<0327:TMFTSN>2.0.CO;2.

Wakabayashi, J., and Sawyer, T.L., 2001, Stream incision, tectonics, uplift, and evolution of topography of the Sierra Nevada, California: Journal of Geology, v. 109, p. 539–562, doi:10.1086/321962.

Wernicke, B., Axen, G.J., and Snow, J.K., 1988, Basin and Range extensional tectonics at the latitude of Las Vegas, Nevada: Geological Society of America Bulletin, v. 100, p. 1738–1757, doi:10.1130/0016-7606(1988)100<1738:BARETA>2.3.CO;2.

Wesnousky, S.G., 2005, Active faulting in the Walker Lane: Tectonics, v. 24, 35 p., doi:10.1029/2004TC001645.

Wesnousky, S.G., Bormann, J.M., Kreemer, C., Hammond, W.C., and Brune, J.N., 2012, Neotectonics, geodesy, and seismic hazard in the northern Walker Lane of Western North America: Thirty kilometers of crustal shear and no strike-slip?: Earth and Planetary Science Letters, v. 329–330, p. 133–140, doi:10.1016/j.epsl.2012.02.018.

Zijderveld, J.D.A., 1967, AF demagnetization of rocks: analysis of results, *in* Collinson, D.W., et al., eds., Methods of palaeomagnetism: Amsterdam, Elsevier, p. 254–286.